Topological Hall effect due to itinerant electrons in a honeycomb skyrmion crystal

A project report

submitted in partial fulfillment for the award of the degree of

Master of Science in Physics

by

Satheesh D M (PH22C043)

under the guidance of

Prof. Birabar Ranjit Kumar Nanda

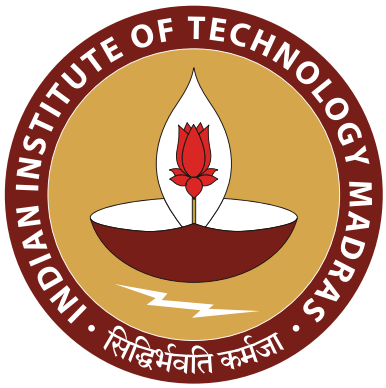

Department of Physics

Indian Institute of Technology Madras

Chennai 600036, India

May 2024

CERTIFICATE

This is to certify that the thesis titled **"Topological Hall effect due to itinerant electron in a honeycomb skyrmion crystal"**, done by **SATHEESH D M (PH22C043)**, is a bona fide record of the work done by him under my supervision. The contents of this project report, in full or in parts, have not been submitted to any other Institute or University for the award of any degree or diploma.

Dr. Birabar Ranjit Kumar Nanda,
Professor,
Department of Physics,
IIT - Madras,
Chennai - 600036.

Place : IITM, Chennai.
Date : 17/05/2024

ACKNOWLEDGEMENT

I owe my deep appreciation and sincere gratitude to Prof. BRK Nanda for supervising my project work and giving me valuable guidance and constructive suggestions to complete this work. I also like to thank my classmate Chethan S (PH22C017) for collaborating with me in this work. Further I also thank the members from Prof Nanda's lab, Arijit Mandal and Pratik Sahu for their feedback and technical support troughout this work. Finally I extend my special thanks to my friends John Paul J and Ganapathy S for encouraging and providing me moral support during the course of work.

Satheesh D M
(PH22C043)

LIST OF ABBREVIATION

SkX	-	Skyrmion Crystal
HE	-	Hall Effect
QHE	-	Quantum Hall Effect
IQHE	-	Integer Quantum Hall Effect
AHE	-	Anamolous Hall Effect
QAHE	-	Quantum Anamalous Hall Effect
THE	-	Topological Hall Effect
SOC	-	Spin-orbit coupling
DMI	-	Dzyaloshinskii - Moriya interaction

ABSTRACT

The SkX exhibits topological Hall effect (THE). Which is its one of its major characteristics. In this thesis the unconventional quantization of the topological Hall conductivity in the honeycomb SkX is studied. Simply, the itinerant electron experiences an emergent inhomogeneous magnetic field due to the spin texture of the skyrmions. This is responsible for the topological Hall effect. The mapping between the THE to the QHE is highlighted. Here, each electronic band from the SkX is understood as a Landau level when they are away from the van Hove singularity. This mapping of THE to QHE aids us in the process of explaining the unconventional behavior of the electrons in SkXs. For example, a skyrmion crystal on a honeycomb lattice exhibits a quantized topological Hall conductivity with steps of 2 e^2/h between the two van Hove singulatities and with steps of e^2/h in the other regions. Also, the conductivity shows a sign change at the van Hove singularity points and at the Dirac point. These unconventional features are linked with the topology of the structural honeycomb lattice. Later the emergent magnetic field is made less inhomogeneous by considering an applied electric field. And it is physically implemented by adding the Rashba and Dresselhaus SOC to the model.

Contents

Chapter 1

Introduction

The investigation of new novel quantum phenomena expands our knowledge boundaries in understanding the physics. One among these phenomena is the THE. It is a perfect example for the manifestation of topology in condensed matter systems. THE is an electrical transport phenomena of a systems with non trivial chiral spin textures like the magnetic skyrmions. Recent discoveries suggest that in topological insulator based magnetic heterostructures, THE is present. The strong SOC and the broken inversion symmetry in such heterostructures could lead to a sizable DMI, which favors the skyrmion stabilization and distinct THE[1]. But, the interesting interplay between the topological surface state (TSS) and THE is yet to be fully understood.

Since discoverd in 2009-10, magnetic textures have become a centre of attraction in physics research and in search for new spintronic technology. This has leading to many fundamental understanding in topology and spin textures. THE signatures help in experimentally classifying the skyrmions. Spintronic devices based on magnetic skyrmions offer several advantages, such as high density and energy-efficient magnetic data storage. This is due to their nanoscale dimensions and topological protection. Magnetic skyrmions can be driven with extraordinarily low current. These charcateristics make them highly promising for data storage and computing applications. Some of the on going research topics include the racetrack memory storage devices, skyrmion based transistors, bio inspired skyrmion based neuromorphic synapse used in neuromorphic computing. Further exploratory research is being done in the aspects of developing skyrmion based qbits for quantum computing applications and in magnetic nanostructure based unconventional computing[1]. This serves as the strong motivation for pursuing this project.

This project seeks to explore into the fascinating realm of topological Hall effect in a skyrmion crystal. Our primary focus will be on numerical investigations of THE in honeycomb SkX. The methodology used here to achieve this goal is to study the energy resolved transverse hall conductivity from a tight binding approximation framework. The TB based model studied here is elementary with only s atomic orbitals, but with the spin degree of freedom. The numerical implementation is

done by using our own code written in python and mathematica softwares.

This project report is organized into several chapters, beginning with a review of the theoretical framework underlying adiabatic transport in a quantum system covering the ideas of geometrical Berry phase in chapter 2. In chapter 3 covers the additional theoretical background in magnetic skyrmions and QHE phenomena. Chapter 4 discusses the problem of electron transport in a skyrmion crystal. Further The effects of Rashba and Dresselhaus spin orbit couplings are introduced. The flow and demonstration of our code is available in this chapter. Chapter 5 discusses the results obtained in the numerical analysis. Followed by the summary and future extensions of this project in chapter 6.

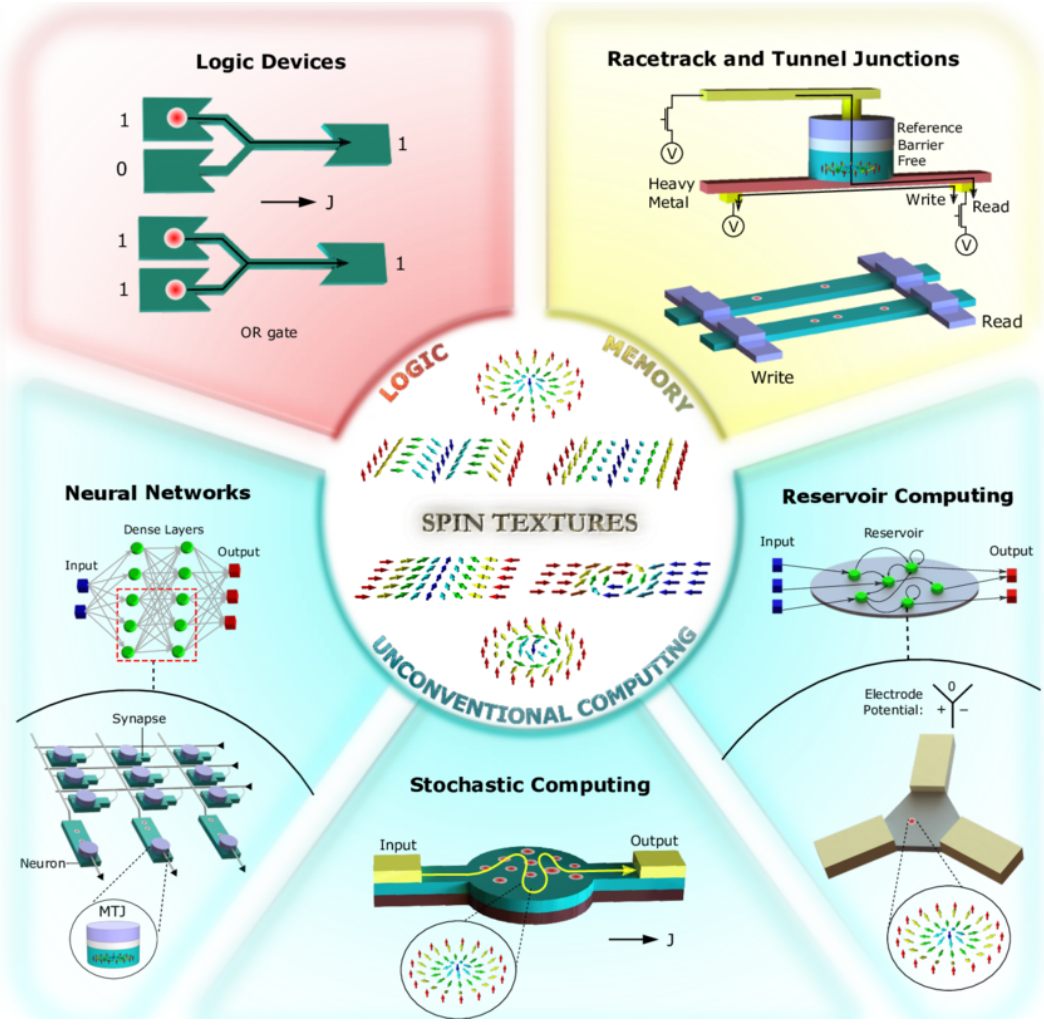

Figure 1.0.1: Mind map explaining the ongoing research based on non trivial spin textures and magnetic skyrmions. Image credits[2].

Chapter 2

Topology & Band Structure Theory

In this chapter the adiabatic transport and the concept of geometrical Berry phase, Berry potential and Berry curvature are reviewed in the initial sections. Later these concepts are applied for an itinerant Bloch electron in a periodic crystal leading to non trivial topology. Then the concept of Chern numbers for such non trivial topology is dicussed.

2.1 Adiabatic theorem and Berry Phase

In quantum mechanics, geometrical phase is the phase acquired by the system's state when it is made to slowly go along a closed circuit in the parameter space of the Hamiltonian. This phenomena was discovered with respect to interference in classical optics by **S. Pancharatnam in 1956**. Later M V Berry generalized this concept for quantum systems **in 1983**. The following derivation of the adiabatic theorem is from Berry's work. [3] [4]

Consider a general hamiltonian, $\hat{\mathcal{H}} = \hat{\mathcal{H}}(\vec{R})$. Such that $\vec{R}$ be a vector parameter. The time evolution of the hamitonian is due to dependence of the vector parameter on time, $\vec{R} = \vec{R}(t)$. So initially it will obey the stationary Schrodinger equation,

$$\hat{\mathcal{H}}(\vec{R}) \left|\Phi_n(\vec{R})\right\rangle = E_n(\vec{R} \left|\Phi_n(\vec{R})\right\rangle \tag{2.1.1}$$

here $\left|\Phi_n(\vec{R})\right\rangle$ are stationary eigenkets of $\hat{\mathcal{H}}$. Adiabatic approximation states that, the when a system evolves slowly then ($t_{ext} >> t_{int} \equiv \frac{E_{ab}}{\hbar}$) the final state is related to its initial state as follows,

$$\left|\Psi_n(\vec{R}(t))\right\rangle = \exp\left\{\frac{-i}{\hbar}\int_0^t E_n(\vec{R}(t'))dt'\right\} \exp\{i\gamma_n(t)\} \left|\Phi_n(\vec{R}(t))\right\rangle \tag{2.1.2}$$

where the first factor is the usual dynamic phase factor, then $\gamma_n(t)$ is the Geometric phase. The

proof of the adiabatic theorem is stated below. Time dependent schrodinger equation states the evolution of the system at all time.

$$\hat{\mathcal{H}}(\vec{R}(t))\left|\Psi_n(\vec{R}(t))\right\rangle = i\hbar\frac{d}{dt}\left|\Psi_n(\vec{R}(t))\right\rangle \tag{2.1.3}$$

Try the following ansartz wave function, where $c(t)$ is due to the time dependence of $\vec{R}$.

$$\left|\Psi_n(\vec{R}(t))\right\rangle = c(t)\exp\left\{\frac{-i}{\hbar}\int_0^t E_n(\vec{R}(t'))dt'\right\}\left|\Phi_n(\vec{R}(t))\right\rangle \tag{2.1.4}$$

Substituting equation 2.1.4 in equation 2.1.3 and solving one can get,

$$\dot{c}(t)\left|\Phi_n(\vec{R}(t))\right\rangle + c(t)\nabla_{\vec{R}}\left|\Phi_n(\vec{R}(t))\right\rangle = 0 \tag{2.1.5}$$

multiply $\left\langle\Phi_n(\vec{R}(t))\right|$ on both sides of the equation 2.1.5 to get,

$$\dot{c}(t) = i\gamma_n(t)c(t) \tag{2.1.6}$$

where, the Geometrical phase is identified as,

$$\gamma_n(t) = \left\langle\Phi_n(\vec{R}(t))\right| i\nabla_{\vec{R}}\left|\Phi_n(\vec{R}(t))\right\rangle \tag{2.1.7}$$

then the factor $c(t)$ can be found by solving equation 2.1.6, this completes the proof of equation 2.1.2.

$$c(t) = \exp\{i\gamma_n(t)\} \tag{2.1.8}$$

Let the system evolves on a closed circuit C in parameter space then the Berry phase over C is,

$$\gamma_n(C) = \oint_C \left\langle\Phi_n(\vec{R}(t))\right| i\nabla_{\vec{R}}\left|\Phi_n(\vec{R}(t))\right\rangle .d\vec{R} \tag{2.1.9}$$

2.1.1 Berry Connection

The integrand of equation 2.1.9 is called the Berry potential or Berry connection and it should be always real since Berry phase is a measurable quantity,

$$0 = \nabla_{\vec{R}}(1) = \nabla_{\vec{R}}\left\langle\Phi_n(\vec{R}(t))\middle|\Phi_n(\vec{R}(t))\right\rangle \tag{2.1.10}$$

$$0 = \left\langle\nabla_{\vec{R}}\Phi_n(\vec{R}(t))\middle|\Phi_n(\vec{R}(t))\right\rangle + \left\langle\vec{R}(t))\middle|\nabla_{\vec{R}}\Phi_n(\Phi_n\vec{R}(t))\right\rangle \tag{2.1.11}$$

$$\left\langle \nabla_{\vec{R}}\Phi_n(\vec{R}(t))\middle|\Phi_n(\vec{R}(t))\right\rangle = \left\langle \Phi_n(\vec{R})\middle|\nabla_{\vec{R}}\middle|\Phi_n(\vec{R})\right\rangle^* = -\left\langle \Phi_n\vec{R})\middle|\nabla_{\vec{R}}\middle|\Phi_n(\vec{R})\right\rangle \tag{2.1.12}$$

The berry connection over C is,

$$\vec{A}_n(C) = \left\langle \Phi_n(\vec{R}(t))\middle| i\nabla_{\vec{R}}\middle|\Phi_n(\vec{R}(t))\right\rangle \tag{2.1.13}$$

2.1.2 Berry Curvature

Berry connection is not guage invariant and it can be easily seen by making a generalised guage transformation with some extra phase $b(\vec{R})$. So that $\left|\Phi_n(\vec{R}(t))\right\rangle \longrightarrow \exp\left\{ib(\vec{R})\right\}\left|\Phi_n(\vec{R}(t))\right\rangle$. Now Berry connection behaves as follows,

$$\vec{A}_n(t) \longrightarrow \vec{A}'_n(t) = \vec{A}_n(t) - \nabla_{\vec{R}}b(\vec{R}) \tag{2.1.14}$$

It will be better to work with guage invariant quantity. So curl of $\vec{A}_n(t)$ is considered, which will be guage invariant. Since, $\nabla_{\vec{R}} \times \nabla_{\vec{R}}b(\vec{R}) = 0$. This quantity is called the Berry curvature,

$$\Omega_n(\vec{R}) := \nabla_{\vec{R}} \times \vec{A}_n(\vec{R}) = i\left\langle \nabla_{\vec{R}}\Phi_n(\vec{R})\middle| \times \middle|\nabla_{\vec{R}}\Phi_n(\vec{R})\right\rangle \tag{2.1.15}$$

The behaviour of Berry connection and Berry potential is analogous to that of magnetic vector potential and magnetic field from electrodynamics. The form of equation 2.1.15 is not suitable for numerical calculations. We will rewrite it so that it depends on the derivatives of Hamiltonian, which can be applicable for most forms of the Hamiltonian. Consider an arbitrary surface S enclosed by the closed circuit C in parameter space of $\hat{\mathcal{H}}$, then by using Stokes theorem,

$$\gamma_n(C) = \oint_C \left\langle \Phi_n(\vec{R}(t))\middle| i\nabla_{\vec{R}}\middle|\Phi_n(\vec{R}(t))\right\rangle .d\vec{R} \tag{2.1.16}$$

$$= \iint_S \Omega_n(\vec{R}) \times d\vec{S} = \iint_S i\left[\left\langle \nabla_{\vec{R}}\Phi_n(\vec{R})\middle| \times \middle|\nabla_{\vec{R}}\Phi_n(\vec{R})\right\rangle\right] .d\vec{S} \tag{2.1.17}$$

$$= \iint_S i\sum_m \left[\left\langle \nabla_{\vec{R}}\Phi_n(\vec{R})\middle|\Phi_m(\vec{R})\right\rangle \times \left\langle \Phi_m(\vec{R})\middle|\nabla_{\vec{R}}\Phi_n(\vec{R})\right\rangle\right] .d\vec{S} \tag{2.1.18}$$

We will see that m = n terms vanish because equation 2.1.11 states that it will give imaginary contribution to the berry phase. Now applying $\nabla_{\vec{R}}$ in equation 2.1.1, we get,

$$\nabla_{\vec{R}}\left[\hat{\mathcal{H}}(\vec{R})\left|\Phi_n(\vec{R})\right\rangle\right] = \left[E_n(\vec{R}\left|\Phi_n(\vec{R})\right\rangle\right] \tag{2.1.19}$$

$$\nabla_{\vec{R}}\left[\hat{\mathcal{H}}\right]|\Phi_n\rangle + \hat{\mathcal{H}}\nabla_{\vec{R}}\left[|\Phi_n\rangle\right] = \nabla_{\vec{R}}\left[E_n\right]|\Phi_n\rangle + E_n\nabla_{\vec{R}}\left[|\Phi_n\rangle\right] \tag{2.1.20}$$

now multiplying $\left\langle \Phi_m(\vec{R}(t)) \right|$ on both sides of the above equation and on simplifying we get,

$$\left\langle \Phi_m(\vec{R}(t)) \right| \nabla_{\vec{R}} \left| \Phi_n(\vec{R}) \right\rangle = \frac{\left\langle \Phi_m(\vec{R}(t)) \right| \nabla_{\vec{R}} \hat{\mathcal{H}} \left| \Phi_n(\vec{R}) \right\rangle}{E_n - E_m} \tag{2.1.21}$$

substituting equation 2.1.21 in equation 2.1.18 we get the final expression for the Berry curvature as,

$$\Omega_n(\vec{R}) = i \sum_{m \neq n} \frac{\left\langle \Phi_n(\vec{R}) \right| \nabla_{\vec{R}} \hat{\mathcal{H}} \left| \Phi_m(\vec{R}) \right\rangle \times \left\langle \Phi_m(\vec{R}) \right| \nabla_{\vec{R}} \hat{\mathcal{H}} \left| \Phi_n(\vec{R}) \right\rangle}{(E_n(\vec{R}) - E_m(\vec{R}))^2} \tag{2.1.22}$$

This equation will be used in numerical calculation of Berry curvature. Due to $E_n(\vec{R}) - E_m(\vec{R}$ in the denominator, the value becomes large when the enargy gap between two leevels are small. and it diverges for degenerate states.

2.2 Topology in Band Structure Theory

The concepts of Geometric phase, Berry connection and Berry curvature were reviewed for any general Hamiltonian in the previous section. In this section these quantities are derived for any solid state physics system with periodic structure. It will become evident that the wave vector $\vec{k}$ plays the vital role of the vector parameter $\vec{R}$ for any periodic crystals.

Now, substituting the Bloch wavefunction (equation **??**) into the time independent Schrodinger equation and multiplying $e^{-i\vec{k}.\vec{r}}$ on both sides we will get,

$$e^{-i\vec{k}.\vec{r}} \hat{\mathcal{H}} e^{i\vec{k}.\vec{r}} U_{n,\vec{k}}(\vec{r}) = E_{n,\vec{k}} U_{n,\vec{k}}(\vec{r}) \tag{2.2.1}$$

equation 2.2.1 is the new form of the Schrodinger equation with the same eigenvalues as before. But the new eigenstates is just the periodic part of the Bloch wavefunction. The new hamiltonian $\hat{\mathcal{H}}(\vec{k}) = e^{-i\vec{k}.\vec{r}} \hat{\mathcal{H}} e^{i\vec{k}.\vec{r}}$ has $\vec{k}$ as its parameter and it the reciprocal space Hamiltonian. From the section 2.1 it can be shown that in the reciprocal space,

$$\gamma_n(C) = \oint_C \left\langle U_{n,\vec{k}}(\vec{r}) \right| i\nabla_{\vec{k}} \left| U_{n,\vec{k}}(\vec{r}) \right\rangle .d\vec{k} \tag{2.2.2}$$

$$\vec{A}_n(\vec{k}) = \left\langle U_{n,\vec{k}}(\vec{r}) \right| i\nabla_{\vec{k}} \left| U_{n,\vec{k}}(\vec{r}) \right\rangle \tag{2.2.3}$$

$$\Omega_n(\vec{k}) = \nabla_{\vec{k}} \times \vec{A}_n(\vec{k}) = i \left\langle \nabla_{\vec{k}} U_{n,\vec{k}}(\vec{r}) \right| \times \left| \nabla_{\vec{k}} U_{n,\vec{k}}(\vec{r}) \right\rangle \tag{2.2.4}$$

This emphasizes that the concept of Berry phase plays a vital role in solid state physics in determining

various quantities. Because it is connected naturally to the band structure.

2.2.1 Bloch electrons in magnetic field

This approach is very close to the tight binding approach of an electron in a periodic lattice[5]. The effect of the external magnetic field can be modeled as an additional phase factor contributing to the hopping parameter of the usual tight binding model under this approach. Consider a 2D system of free electrons which are invariant under translation symmetry. Let $\hat{T}_{\vec{R}}$ be the translation operator. Here $\vec{R}$ is the lattice translation vector. Then,

$$\hat{T}_{\vec{R}} e^{i\vec{k}.\vec{r}} = e^{i\vec{k}.\vec{R}} e^{i\vec{k}.\vec{r}} \tag{2.2.5}$$

$$\hat{T}_{\vec{R}} = \exp\left\{ i\frac{\vec{p}.\vec{R}}{\hbar} \right\} \tag{2.2.6}$$

Here $\hat{T}_{\vec{R}}$ will commute with the hamiltonian of a electron in a lattice system, then it can be claimed that both the operators share the diagonal form in some common basis. Now consider the same electron in a lattice system in magnetic field then,

$$\hat{\mathcal{H}} = \frac{1}{2m}\left[\hat{\vec{p}} + e\vec{A}\right]^2 + V(\vec{r}) \tag{2.2.7}$$

Now $\hat{T}_{\vec{R}}$ will not commute with the hamiltonian as the cyclotron motion does not allow the momentum to be conserved. So we will consider modification to the translation operator by replacing $\vec{p} \longrightarrow \hat{\vec{p}} + e\vec{A}$ and call it the magnetic translation operator. In the symmetric guage $\vec{A} = \vec{r} \times \vec{B}/2$,

$$\hat{T}_{\vec{B},\vec{R}} = \exp\left\{ \frac{i}{\hbar}\vec{R}.\left[\hat{\vec{p}} + \frac{e}{2}(\vec{r} \times \vec{B})\right] \right\} = \hat{T}_{\vec{R}} \exp\left\{ \frac{ie}{\hbar}(\vec{B} \times \vec{R}).\frac{\vec{r}}{2} \right\} \tag{2.2.8}$$

Here the magnetic translation operator will commute with the hamiltonain in equation 2.2.7. Consider two translation vectors $\vec{R}_a$ and $\vec{R}_b$ so the commutation relation between two magnetic translation operators is given by,

$$\left[\hat{T}_{\vec{B},\vec{R}_a}, \hat{T}_{\vec{B},\vec{R}_b}\right] = (e^{2\pi i\phi} - 1)\hat{T}_{\vec{B},\vec{R}_b}\hat{T}_{\vec{B},\vec{R}_a}, \qquad \phi = \frac{eB}{h}ab \tag{2.2.9}$$

where ϕ is the number of flux quantum through the cell defined by $\vec{R}_a$ and $\vec{R}_b$. Then these operators commute only when $\phi \in Z$. Consider a magnetic unit cell which is now defined by the vectors $q\vec{a}$

and $\vec{b}$ where $\vec{a}$, $\vec{b}$ the original unit vectors of the lattice. Then the magnetic lattice vector is given by,

$$\vec{R'} = n(q\vec{a}) + m(\vec{b}) \tag{2.2.10}$$

Then the flux through this magnetic unit cell be p (integer) times the flux quantum (h/e). So $\Phi/\Phi_o = p/q$ where Φ_o is the flux through unit cell of the lattice. Let $|\psi\rangle$ be the eigenstate of both $\hat{\mathcal{H}}$ and $\hat{T}_{\vec{B},\vec{R}}$ Then for the unit vector translations of the magnetic unit cell,

$$\hat{T}_{\vec{B},q\vec{a}}\,|\psi\rangle = e^{iq\vec{a}.\vec{k}_1}\,|\psi\rangle\,, \qquad \hat{T}_{\vec{B},\vec{b}}\,|\psi\rangle = e^{i\vec{b}.\vec{k}_2}\,|\psi\rangle \tag{2.2.11}$$

where, k_1 and k_2 are the generalized crystal momentum which are uniquely restricted to the brillouin zone ($0 \leq k_1 \leq 2\pi/qa$ and $0 \leq k_2 \leq 2\pi/b$). Then the Bloch wavefunction for band n is given by,

$$|\Psi_{k_1,k_2,n}(\vec{r})\rangle = e^{i\vec{k}_1.\vec{r}}e^{i\vec{k}_2.\vec{r}}U_{k_1,k_2,n} \tag{2.2.12}$$

The reciprocal space wavefunction in polar form is given by,

$$U_{\vec{k}} = |U_{\vec{k},n}|e^{i\phi_{\vec{k},n}(\vec{r})} \tag{2.2.13}$$

then the integer p is related to the phase $\theta_{\vec{k}}$ as the integration over the magnetic unit cell in counter clockwise direction. This quantity is called the Chern number or topological invariant of the band.

$$C_n = \frac{1}{2\pi}\oint_C dl.\frac{\partial}{\partial l}\phi_{\vec{k},n}(\vec{r}) \tag{2.2.14}$$

2.2.2 Chern number

Chern number associated with this structure is also defined as the sum of the Berry fluxes over the plaquettes of a closed surface forming a torus.

$$\gamma_n(C) = \oint_C \vec{A}_n.d\vec{R} = \iint_{S_1}\Omega_n(\vec{R}).d\vec{S} + 2\pi p = \iint_{S_2}\Omega_n(\vec{R}).d\vec{S} + 2\pi p' \tag{2.2.15}$$

where S_1 and S_2 are different surfaces and their combined seam is C shown in the figure below. Derviation and realization of the Chern theorem is beyond Then Berry curvature over the entire surface is,

$$\frac{1}{2\pi}\iint_S \Omega_n(\vec{R}).d\vec{S} = \frac{1}{2\pi}\left[\iint_{S_1}\Omega_n(\vec{R}).d\vec{S} - \iint_{S_2}\Omega_n(\vec{R}).d\vec{S}\right] \tag{2.2.16}$$

$$= \frac{1}{2\pi}[\gamma_n(C) - 2\pi p' - \gamma_n(C) + 2\pi p] = p - p' = C_n \in Z \tag{2.2.17}$$

$$C_n \equiv \frac{1}{2\pi} \iint_S \Omega_n(\vec{R}).d\vec{S} \tag{2.2.18}$$

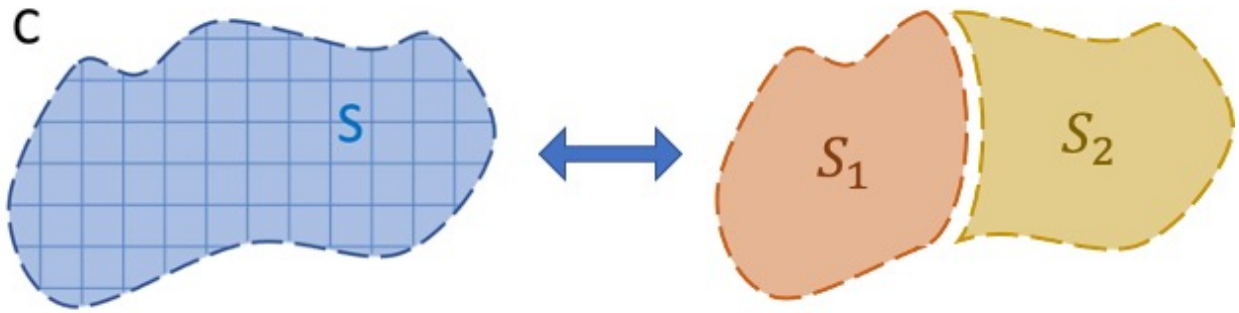

Chapter 3

Theoretical Background

The theoretical background of magnetic skyrmions and various QHE are discussed here.[6][7]

3.1 Micromagnetism

In this section, we discuss the theory of micromagnetism. Micromagnetism is a theory which studies the the phenomena of magnetism in a larger length scale when compared to underlying atomic lengths. So the atomic structure of each and every atom in the system can be ignored. The quantity of interest here is the magnetic moment. Atoms are associated with magnetic moment vectors and their interaction within the system considered in this theory. The system considered here will be a general lattice structure representing a condensed matter with magmetic moments at each site. The interactions between the magnetic moments are capable of explaining creation of the long range ordering in the system and existence of various exotic magnetic states like magnetic vortexes, helical state, skyrmions etc.

Magnetic moment

In the classical electromagnetism, the magnetic moment of a current carring loop is given by,

$$\vec{\mu} = I \int_A d\vec{A} \tag{3.1.1}$$

here, I is the current through the loop and A is the area enclosed by the loop. Where the current direction determines the direction of the moment and it is always normal to the surface enclosed. The origin of magnetic moments in a atom is mainly associated with the motion of electrons around the nucleus (orbital motion contribution) and their spin. The quantity spin and orbital angular momentum are purely quantum mechanical and it is often misunderstood that the electrons actually

spin or revolves about an axis. But this is a misnomer, they behave as if a classical spinning or revolving object. The evidence is that the subatomic particles behave like a bar magnet, and this bar magnet kind of behaviour is observed in current carrying loop. The magnetic moment of the atom is given by,

$$\vec{\mu} = g\mu_B \vec{S} \tag{3.1.2}$$

$$g = 1 + \frac{J(J+1) - L(L+1) + S(S+1)}{2J(J+1)} \tag{3.1.3}$$

where, g is called the gyromagnetic ratio and $\vec{S}$ is the total spin angular momentum of the electrons in an atom and μ_B is the Borh magneton. So magnetic moment is the basic unit in this theory.

3.1.1 Heisenberg exchange interaction

This interaction is strong when compared to the other interactions to be discussed. At the same time it is a short range interactions. This interaction originates from the overlap of electron orbitals, and first proposed by Heisenberg. Later Dirac showed from the symmetry arguments that the interaction energy between any two spins in the lattice is given as $-2J_{ij}\vec{S}_i.\vec{S}_j$. So the total exchange interaction energy is given by,

$$\mathcal{H}_{exchange} = -\sum_{<ij>} J_{ij}\vec{S}_i.\vec{S}_j \tag{3.1.4}$$

the summation is always over a pair of neighbouring moments at sites i and j and denoted by $< ij >$ in the summation. Then i and j runs from site 1 to site N in the system. When isotropic exchange interactions are assumed then for all the NN pairs the $J_{ij} = J_{ex} = J_1$, similarly for the second NN it will be some constant J_2 and so on. When $J_{ij} > 0$ it favours parallel alignment of spins which explains ferromagnetism. If $J_{ij} < 0$ it favours parallel alignment of spins thus explaining anti-ferromagnetism. Thus accomodating all the coplanar long range ordering in the picture.

This exchange interaction can also give rise to non coplanar spin ordering, When competing interactions with both ferromagnetic and antiferromagnetic neighbour couplings are considered. Also geometry frustrations like antiferromagnetic NN exchange in triangular lattice will also result non coplanar spin ordering.

3.1.2 Zeeman interaction

This is the interaction of the system with the external magnetic field $\vec{B}$. The external field breaks the symmetry in the system and favours the alignment of spins in the direction of the external field. This is expressed as,

$$\mathcal{H}_{zeeman} = -g\mu_B \sum_i \vec{B}.\vec{S}_i \tag{3.1.5}$$

3.1.3 Magnetocrystalline anisotropy

In crystal systems, it takes different energires to magnetise the system along diferent directions. This effect is called the magnetocrystaline anisotropy. The direction which minimizes the energy is called the easy axis of the crystal. The origin of this anisotropy is due to the interactions between the spin, orbital angular momentum of the electrons and with the lattice. So these are the possible degrees of freedom for magnetocrystaline anisotropy. The stong reason is due to the quenching of electron orbital in a crystal. This quenching occurs because of the presence of crystal field. But the physical origin stems from the spin obit coupling (SOC). The quenched electron orbitals, they tend to reorient the spins via SOC. This term is mathematically given by,

$$\mathcal{H}_{anisotropy} = -K \sum_i (\vec{S}_i.\hat{e}_{an})^2 \tag{3.1.6}$$

here $\hat{e}_{an}$ gives the easy axis direction. K (> 0) is the anisotropy strength. Similar to the Zeeman field this also breaks the symmetry in the system and favours the easy axis alignment when considerd.

3.1.4 Dipole - dipole interaction

This term gives the contribution to the total energy due to the interaction between magnetic dipoles. This interaction is due to the presence of the magnetic moment at site i in the induced magnetic field of the another moment at site j. This a long range interaction, when compared to all other interactions in this model. This interaction favours the attraction of the north and south poles the interacting magnetic moments. Despite being weaker than the exchange interaction, over long distances it becomes the dominating interaction. This behavior will also result in the stabilization of non-collinear spin ordering. This term is expressed as,

$$\mathcal{H}_{DDI} = -\frac{\mu_o}{4\pi} \sum_{ij} \left(3\frac{(\vec{S}_i.\vec{r}_{ij})(\vec{S}_j.\vec{r}_{ij})}{|\vec{r}_{ij}|^5} - \frac{\vec{S}_i.\vec{S}_j}{|\vec{r}_{ij}|^3} \right) \tag{3.1.7}$$

3.1.5 Dzyaloshinskii - Moriya interaction

Dzyaloshinskii–Moriya interaction (DMI) is also known as antisymmetric exchange interaction. DMI forces the spins of neighboring sites to align perpendicular to each other. This give only canted spin ordered states. The Heisenberg interaction between two spins favors coplanar ordered states, whereas DMI induces a clockwise or counter-clockwise rotation between the spins. DMI also has its physical origin from the SOC of and electron at a particular site. Moriya suggested that the spin interaction prescribed by Dzyaloshinskii must be an antisymmetric interaction taking the form,

$$\mathcal{H}_{DMI} = \sum_{<ij>} \vec{D}_{ij}.(\vec{S}_i \times \vec{S}_j) \tag{3.1.8}$$

here, $\vec{D}_{ij}$ is the DM vector. Moriya arrived at this conclusion by considering a microscopic model of with interaction only between two magnetic metal atoms with only one 3d orbital. The total hamiltonian of this model is,

$$\mathcal{H} = \mathcal{H}_o^i + \mathcal{H}_o^j + T_{ij} + \mathcal{H}_{SOC}^i + \mathcal{H}_{SOC}^j \tag{3.1.9}$$

where, $\mathcal{H}_o^i$ denote the onsite energy of localised 3d electrons at site i. Given in the Hubbard model framework by,

$$\mathcal{H}_o^i = \sum_{m\sigma} \epsilon_{im} \hat{c}_{im\sigma}^\dagger \hat{c}_{im\sigma} + U \sum_{m\sigma \neq m'\sigma'} n_{im\sigma} n_{im'\sigma'} \tag{3.1.10}$$

here, ϵ_{im} is the orbital energy of 3d electron, and U indicates the Coulomb repulsion. T_{ij} is the usual site hopping term. $\mathcal{H}_{SOC}^i$ term represents the SOC at site i with orbital angular momentum $\vec{L}_i$ and spin $\vec{S}_i$. It is given by,

$$\mathcal{H}_{SOC}^i = \xi \vec{L}_i.\vec{S}_i \tag{3.1.11}$$

Under the assumption of the large U limit ($U >> t_{ij}$), the last three terms in the equation 3.1.9 can be treated as the perturbation to $\mathcal{H}_o = \mathcal{H}_o^i + \mathcal{H}_o^j$. To the first order aproximation ($O(\xi^2)$), the effective model now becomes,

$$\mathcal{H}_{eff} = J_{ij}\vec{S}_i.\vec{S}_j + \vec{D}_{ij}.(\vec{S}_i \times \vec{S}_j) + O(\xi^2) \tag{3.1.12}$$

where, the first term is the Heisenberg symmetric exchange interaction term with hopping strength given $J_{ij} = J_{ji} \sim t_{ij}^2/U$. The second term is the antisymmetric exchange interaction term with $D_{ij} = -D_{ji} \sim \xi(t_{ij}^2)/U$.

An intuition for this result can be as follows: In the absence of SOC, the electron hopping between nearest neighbor magnetic atoms does not occur with spin-flipping, and the neighboring spins prefer collinear configuration due to Heisenberg exchange. The spin-flipping hopping process of electrons is a consequence of SOC in the model. This two sites spin-flipping hopping process defines the microscopic origin of DMI.

In this section, various interaction mechanisms in a magnetic system were discussed. The content discussed here belong to the static micromagnetism which captures only the formation of various magnetic phases in a system related to this thesis work. Further there is dynamics micromagnetics expained by the Landau-Lifshitz-Gilbert (LLG) equation.It explains many interesting mechanisms like the spin orbit torque, spin transfer torque, spin hall effect, skyrmion hall effet etc, These are the outcomes of the micromagnetics framework.

3.2 Magnetic Skyrmions

In this section topological protection of the magnetic skyrmions are discussed with respect to their winding numbers. Then classification of skyrmions is discussed. Later a overview on the various stabilization mechanisms are reviewed. It is followed by the mathematical definition of the skyrmion crystal state. Then the experimental obsevations of skyrmions are reviewd from literature.

3.2.1 Topology of Skyrmions

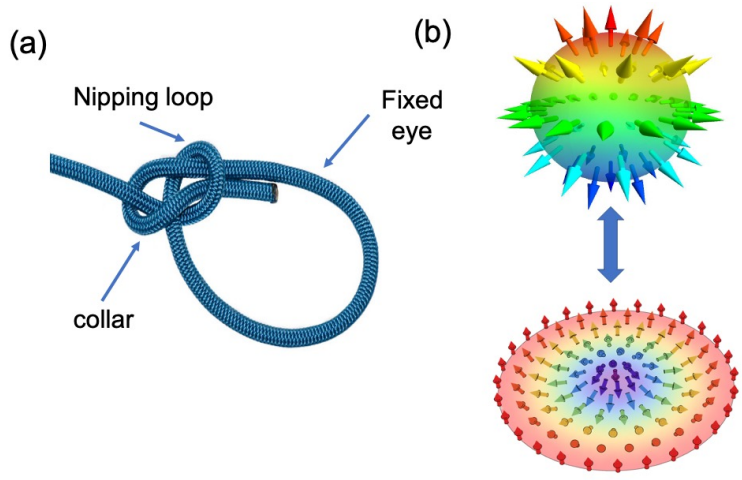

Figure 3.2.1: Non trivial topology. (a) Bowline knot, simple example of a non trivial topology. (b) Stereographic mapping of the Neel type skyrmion onto a 2-Sphere S^2.

Magnetic skyrmions are also known as the magnetic vortex like configurations. These are metastable configurations of magnetic ordering in a uniform magnetic background (ferromagnet).

They are also both theoretically predicted and observed to be from a crystal lattice. Metastability of the magnetic skyrmions are associated with their topological properties. Mathematically, the skyrmion state is charectarised by a topological winding number of skyrmions W_{sk}. The skyrmion charge diffentialtes from the trivial collinear magnetic states (i.e, ferro, antiferro, ferri magnetic states). And it is defined as,

$$W_{sk} = \frac{1}{4\pi} \iint \vec{m}(\vec{r}). \left(\frac{\partial \vec{m}(\vec{r})}{\partial x} - \frac{\partial \vec{m}(\vec{r})}{\partial y} \right) d^2r \tag{3.2.1}$$

here, $\vec{m}(\vec{r})$ is the normalised local spin configurations, often known as the spin texture of a skyrmion. Topological charge take integer values ± 1 for the case of skyrmions. Winding number of a closed path is defined as the number of times the path goes around the point inside the closed path in counter clockwise direction. To understand this, we must focus on the construction of skyrmions. Skyrmionic configuration can be visualised as the sterographic projection of spins from the skyrmionic configuration in 2 dimensions onto the surface of a unit 2-sphere S^2. This mapping explains the non trivial topology of the skyrmions.

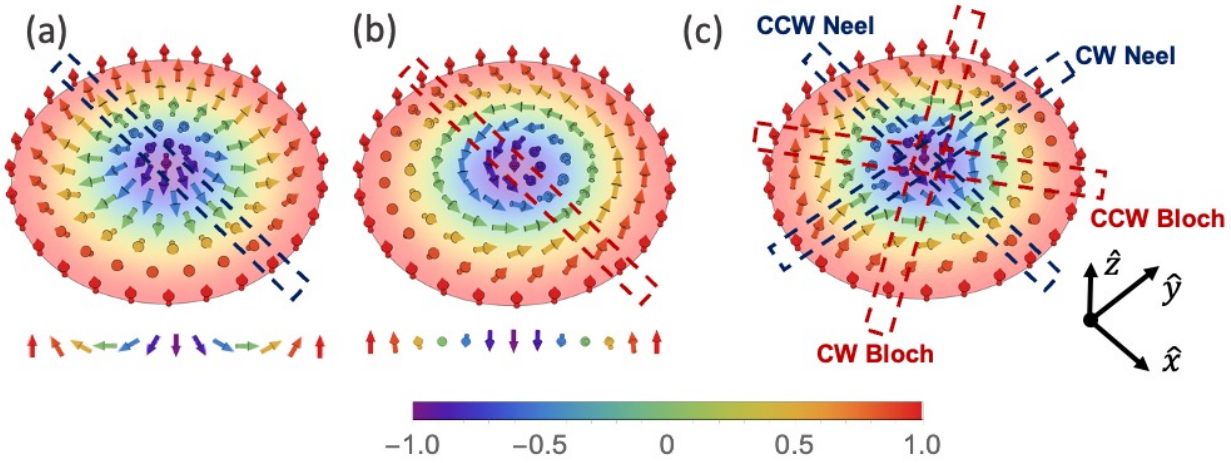

Figure 3.2.2: Anatomy of Skyrmions and Winding numbers. (a) Neel type skyrmion. Cross section along any radial direction is a CCW Neel domain wall. (b) Bloch skyrmion. Cross section along any direction is a CCW Neel domain wall. Both (a), (b) spins wrap around S^2 sphere once. Hence $+1$ winding number. (c) Anti-skyrmion, showing different domain wall type cross sections along different radial directions. Alternates between Neel and Bloch walls with CW and CCW rotation of spins, depending on the skyrmions. The spins at fixed radial distance rotates in clock wise direction when the contour of integration of winding number is in counter clokwise direction. Hence this anti-skyrmion has a winding number of -1.

Non trivial topology is like a knot in a rope and to untie the knot one must use the extremities of the rope. If the rope is forming a closed loop the one must cut the rope. So a continuously transformation of 2 topologically different objects is not possible.

In an ideal infinite magnetic system the configurations are said to be topologically equivalent if there exists a continuous transformation between them without having to overcome an infinite energy barrier. Skyrmions and the collinear magnetic states belong to different topological genus. This offers a stability to Skyrmions. In reality, the magnetic systems are discrete and hence the energy barrier is not infinity but very large value. This is the reason for the skyrmion states being metastable.

3.2.2 Characterization of skyrmions

This section discusses the continuum model of individual skyrmions. When describing a lattice model then the parameters assumes only discrete values. Consider a point in the planar space (X, Y) being parameterized as,

$$X = r\cos(\alpha), \qquad Y = r\sin(\alpha) \tag{3.2.2}$$

Now applying the stereographic mapping on to a unit radius 2-sphere S^2 with coordinates $(1, \theta, \phi)$, Then the corresponding Cartesian components of the 2-sphere spins will give the spin profile of the skyrmion in the continuum model by,

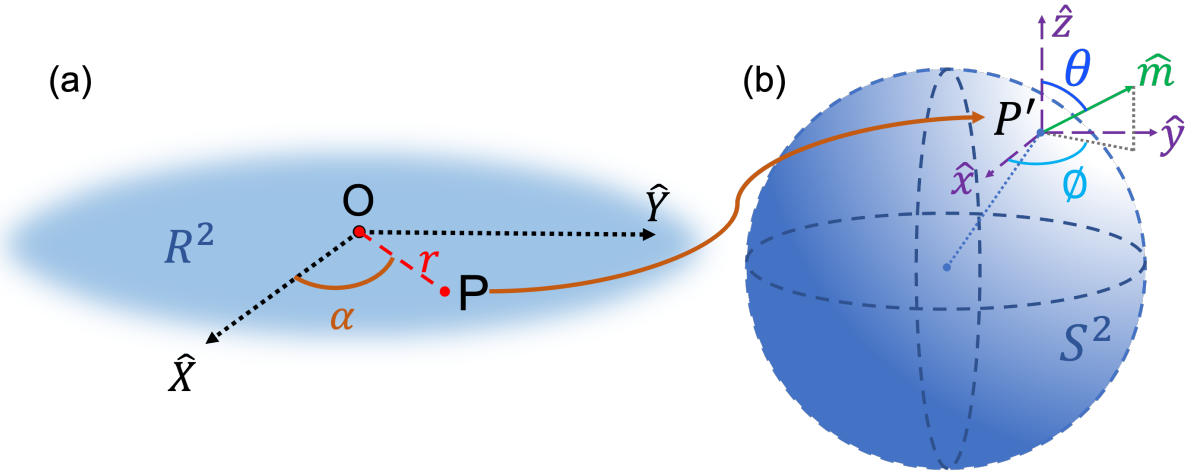

Figure 3.2.3: Coordinate system to describe the stereographic projection in the continuum model of the individual magnetic skyrmion. (a) $(\hat{X}, \hat{Y})$ spans the 2D plane of the skyrmion, R^2. Any point P is given by (r, α). O is the origin representing the centre of skyrmion. The fading blue disc represents the R^2 plane extending to infinity. (b) $(\hat{x}, \hat{y}, \hat{z})$ are the local coordinate directions on the 2-sphere S^2 to represent the local magnetization texture $\vec{m}(\vec{r})$ by mapping $R^2 \longrightarrow S^2$, thus relating the points P and P'. Here the polar angle is only a function of radial coordinate, $\theta(r)$. And the azimuthal angle is only on a function of α, $\phi(\alpha)$.

$$x = \sin\theta\cos\phi = \sqrt{1-\cos\theta}\cos\phi \tag{3.2.3}$$

$$y = \sin\theta\sin\phi = \sqrt{1-\cos\theta}\sin\phi \tag{3.2.4}$$

$$z = \cos\theta \tag{3.2.5}$$

then, the spin profile of the skyrmion is given by,

$$\vec{m}(\theta,\phi) = (\sin\theta\cos\phi, \sin\theta\sin\phi, \cos\theta) \tag{3.2.6}$$

Now substituting equation 3.2.6 in equation 3.2.1, we obtain,

$$W_{sk} = \frac{1}{4\pi}\iint_{S^2}\sin\theta d\theta d\phi = \frac{-1}{4\pi}[\cos\theta]\ \ [\phi] \tag{3.2.7}$$

So, the skyrmion winding number depends on both the parameters defining the contribution of in plane magnetization (ϕ) and out of plane magnetization (θ). Now we are supposed to choose a convention to accommodate both equivalent variations of individual magnetic skyrmions in a ferromagnetic background with spins pointing in both $+\hat{z}$ and $-\hat{z}$ directions.When the background texture points in $+\hat{z}$ direction. It means that as $r \longrightarrow 0$, $\theta \longrightarrow \pi$. Then $[\cos\theta]_{\pi}^{0} = 2$ This results in a winding number,

$$W_{sk}^{\uparrow} = -\frac{1}{2\pi}[\phi] \tag{3.2.8}$$

When the background texture points in $-\hat{z}$ direction. Then $\theta \longrightarrow 0$ as $r \longrightarrow 0$. This will give,

$$W_{sk}^{\downarrow} = \frac{1}{2\pi}[\phi] \tag{3.2.9}$$

In both cases the ϕ limits is over a unit sphere in plane (x, y). Now there are several possibilities for the in plane magnetization. Here we consider a linear variation in ϕ parameterised by two new quantities called the helicity number m, and vorticity number γ.

$$\phi := m\alpha + \gamma \tag{3.2.10}$$

then we also define another quantity called the vorticity number given by,

$$m = \frac{1}{2\pi}[\phi] \tag{3.2.11}$$

Then by equations 3.2.8 and 3.2.9, we get,

$$W_{sk}^{\uparrow} = -m \tag{3.2.12}$$

$$W_{sk}^{\downarrow} = m \tag{3.2.13}$$

then the magnetization profile can be represented in the new parameters as,

$$\vec{m}(m,\gamma) = (\sin\theta\cos(m\alpha+\gamma), \sin\theta\sin(m\alpha+\gamma), \cos\theta) \tag{3.2.14}$$

When the background spin texture is known then the Skyrmion charge is determined by the vorticity number. If we define a quantity call the polarity, denoting the only the direction of spin at the origin. Then the skyrmion charge in general can be defined as the product of the polarity (p) and the vorticity number (m).

$$W_{sk} = pm \tag{3.2.15}$$

skyrmion The helicity number does not play a role in determining the skyrmion charge. It is a measure of the addition twist in the in plane contribution to the magnetization. So any skyrmion is uniquely characterised by the three parameters pair (W_{sk}, m, γ)

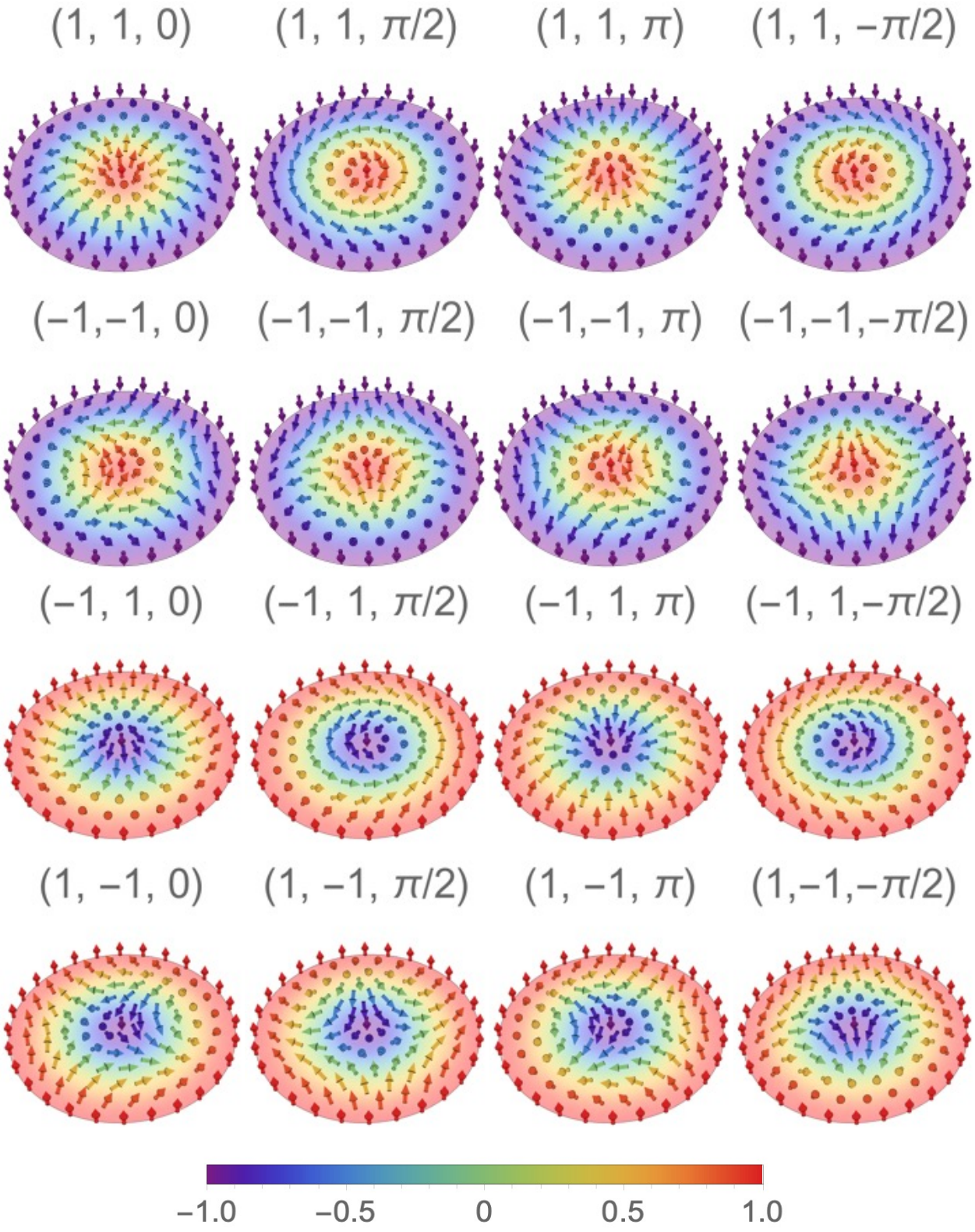

Figure 3.2.4: Classification of skyrmions according to the parameters (W_{sk}, m, γ)

3.2.3 Stabilization of skyrmion

Frustration stabilization mechanism

In a lattice with hexagonal geometry like triangular or honeycomb lattice each atom has six and three nearest neighbors respectively. When a antiferromagnetic Heisenberg coupling is considered, they all would be anti-parallel to the reference moment. Also the pairs of neighbors are nearest neighbors among themselves. Hence they should also align antiferromagnetically according to the Heisenberg interaction, which is not physically possible. Hence the resulting spin arrangement is a compromise of these competing interactions. This non-collinear state originates purely from geometrical frustration. When additional frustration is introduced by considering a ferromagnetic interaction between nearest neighbors J1 $>$ 0 and an antiferromagnetic second-nearest neighbors J2 $<$ 0, this non-collinearity becomes even more preferable. The ground state is a helical spin spiral phase with no net magnetization. Also known as the single-q state.

Another essential contribution is from the application of an external magnetic field B along the direction of the net magnetization of skyrmions (out-of plane). This external field makes the skyrmion state energetically favorable over the helical phase at higher temperatures. The magnetic field is introduced in the Hamiltonian via a Zeeman interaction term as disucssed in section 3.1. Further, easy axis anisotropy also favors moments pointing out-of-plane, as it is typically in the case of thin films. This leads to a further stabilization of magnetic skyrmions. Skyrmions which are stabilized by frustrated exchange have diameters of only a few nanometers. This is due to the strong spin canting.

Other mechanisms

Dipole-dipole interactions stabilizing larger skyrmions and magnetic bubbles of size 100 nm to 1μm. Because these interactions become dominant in long range when compared to the other interactions from section 3.1. In magnetic thin films with perpendicular easy-axis anisotropy, the dipolar interaction prefers an in-plane magnetization, whereas the anisotropy favours an out-of-plane magnetization. The competition between these two interactions results in canted spin texture in the thin film layers. An applied magnetic field perpendicular to the film turns them into a periodic array of magnetic bubbles or skyrmions. DM interaction based mechanism. In non-centrosymmetric materials like the MnSi, FeGe, transformation from the helical spiral (single-$\vec{q}$)into the triangular-lattice skyrmion crystal under an external magnetic field occurs. This mechanism stabilizes skyrmions of size 5 - 100 nm.Further four-spin exchange interactions, which can lead to atomic-sized skyrmion structures has be identified in Fe - Ir interfaces. [1]

3.2.4 Skyrmion crystal state (SkX)

Skyrmion lattice state (SkX) is given by the triple-q state. This triple-q state is a superposition of three distorted spirals characterized by wave vectors $\vec{q}_1$, $\vec{q}_2$, and $\vec{q}_3$ with an additional uniform component along H. In contrast to the single-q and the double-q states, three spiral planes are perpendicular to the xy plane and are rotated by 120 degrees with each other[8]. It is given by,

$$m_{i,xy} = \sum_{j=1}^{3} \sin\left(\vec{q}_j.\vec{r}_i + \theta_j\right)\hat{e}_j \tag{3.2.16}$$

$$m_{i,z} = \sum_{j=1}^{3} \cos\left(\vec{q}_j.\vec{r}_i + \theta_j\right) \tag{3.2.17}$$

here, $\hat{e}_i$ is the direction vector in the xy plane or in the plane of the skyrmion. These indicate the the direction of the spin spirals. And they should be sperated by 120 degrees from each other. This is ensured by the constraint, that sum of these unit vectors should give a null vector. And θ_j ($j \in \{1, 2, 3\}$) is a phase factor satisfying the constraint, $\cos(\theta_1 + \theta_2 + \theta_3) = \pm 1$. (polarity $+1$ or centre spin pointing up and vice versa)

$$\sum_{i=1}^{3} \hat{e}_i = 0; \qquad \sum_{i=1}^{3} \theta_i = \pi \text{ (or) } 2\pi \tag{3.2.18}$$

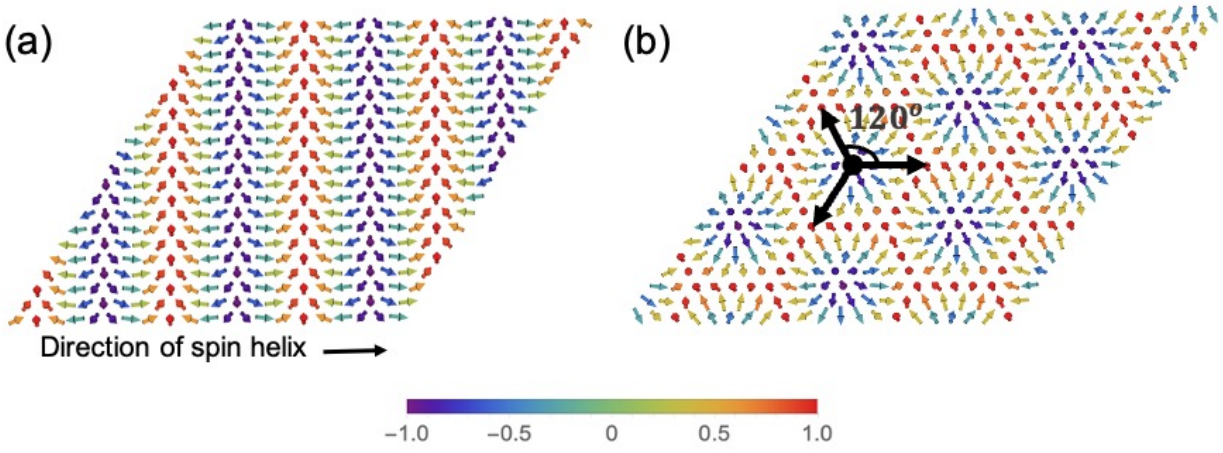

Figure 3.2.5: (a) It is the single-q ground state with no net magnetization. Only one $\vec{q}$ characterizes the spin helix xy component of this state. (b) Skyrmion crystal state or the triple-q state, (Neel skyrmion, m = 1 and $\gamma = 0$) with the arrows denoting the $\hat{e}_i$ direction vectors. It a superposition of three such spin helix textures in (a) along $\hat{e}_i$ directions. This triple-q texture is used in this thesis.

3.2.5 Experimental observations

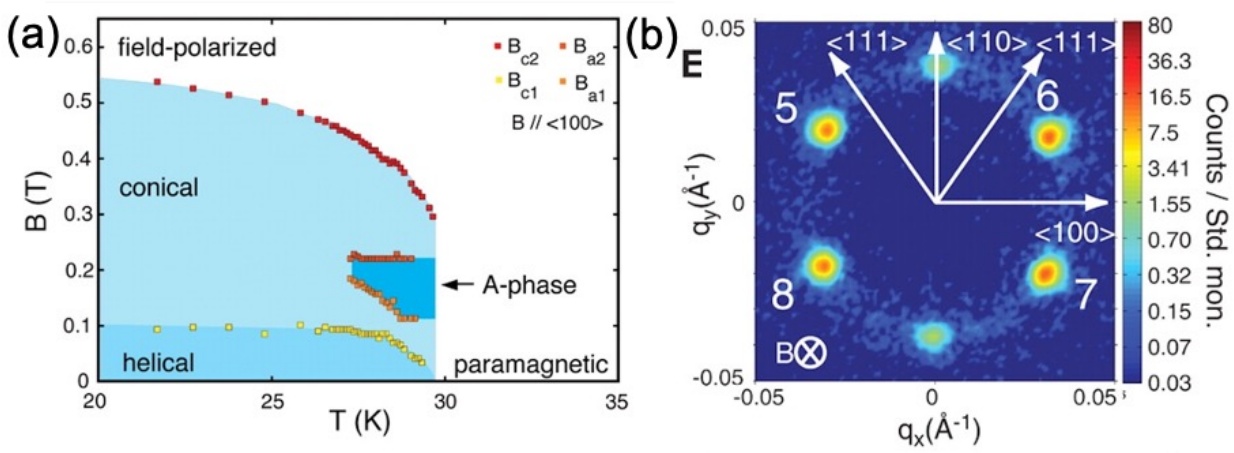

Figure 3.2.6: Initial reciprocal-space observation by Neutron scattering experiment in 2009. (a)The phase diagram of MnSi as a function of T and B. Here the A - phase corresponds to the SkX phase of MnSi. (b) Image of Bragg spots in reciprocal space with six intensity maxima, corresponding to the wave vectors of the three superimposed spin spirals which form a SkX. Image credits: [9]

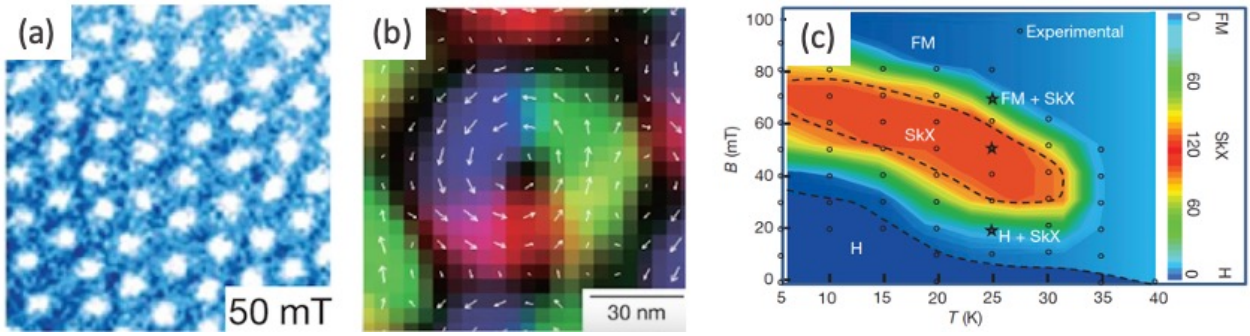

Figure 3.2.7: Real space observation using Lorentz Transmission Electron Microscopy (LTEM) in 2010. (a) Overfocus image of the SkX in $Fe_{0.5}Co_{0.5}Si$ forming a triangular lattice of skyrmions. (b) Processed LTEM image showing a Bloch SkX. The arrows and colors corresponds to the in-plane orientation of the magnetic moments. (c) Phase portrait of $Fe_{0.5}Co_{0.5}Si$. Image Credits: [10]

Further in 2011 Neel type Skyrmion crystal (helicity γ = 0)(forming a triangular lattice) were identified in the Fe-Ir interface by using the SP-SEM. They are induced due to interfacial DM interaction. Further antiskyrmions are obsreved in materials with anisotropic DM interactions[11].

3.3 Quantum Hall Effects

The Hall effect is known as the accumulation of a charge carriers (electrons) across an electrical conductor, that is transverse to the current in the conductor. This effect happens due to magnetic Lorentz force experienced by the charge carriers due to applied magnetic field. Here the applied magnetic field, charge current and the electric field induced due to hall voltage are mutually perpendicular to each other. This interesting effect was discovered by Edwin Hall in 1879.

This effect could be explained successfully in the classical regime using the electrodynamics under the assumptions of the Drude model of conductor. This model states that he Hall coefficient is a characteristic of the conducting material and is given by the ratio of the induced electric field to the product of the current density and the applied magnetic field ($R_H = E_y/(B_z j_x)$). Then the transverse conductivity varies linearly with the applied field. Ans the longitudinal conductivity remaining the same.

The Quantum version of the Hall effect was first observed in a 2D system in a MOSFET at a very low temperature (T $<$ 4 K) and subjected to a strong perpendicular magnetic field in the order of Tesla (T). the electrical conductivity takes on values that are fundamentally different from the predictions of classical physics. Klaus von Klitzing was awarded with the Nobel prize in 1985 for his contribution in relating the fundamental constants with the IQHE. The Hall conductivity takes quantised values ($\sigma_{xy} = ne^2/h$). Topological property of the system plays a vital role when it comes to understanding any quantum version of the Hall effects.

In many ferromagnets the transverse Hall conductivity acquires an additional term independent of the applied magnetic field in 1881 by Hall himself. This term was identified to be proportional to the magnetisation M of the sample. And it becomes constant once the sample has reached its saturation magnetisation. The effect is known as the anomalous Hall effect. While the ordinary Hall effect of explained in classical physics requires an external magnetic field, the anomalous Hall effect requires only a net magnetisation. Analogous quantum version exists for the AHE also. The effect has been observed in a variety of systems, including transition metals and transition metal oxides, in materials with colossal magnetoresistance, ferromagnetic semiconductors, topological insulators and a host of other topological materials showing possibilities of magnetic solitons like Skyrmions, Magnetic bubbles and vortexes etc. And these QAHE and THE has become the recent active topics of research in the past two decades.[12]

In this section we will focus on deriving and understanding the TKNN relation and its connection to the topology of any Quantum Hall system in general. Fisrt we will start with obtaining a formula for the hall conductivity called the Kubo formula. The formulae discussed here will aid in computing the Hall conductivity and understanding the phenomena.

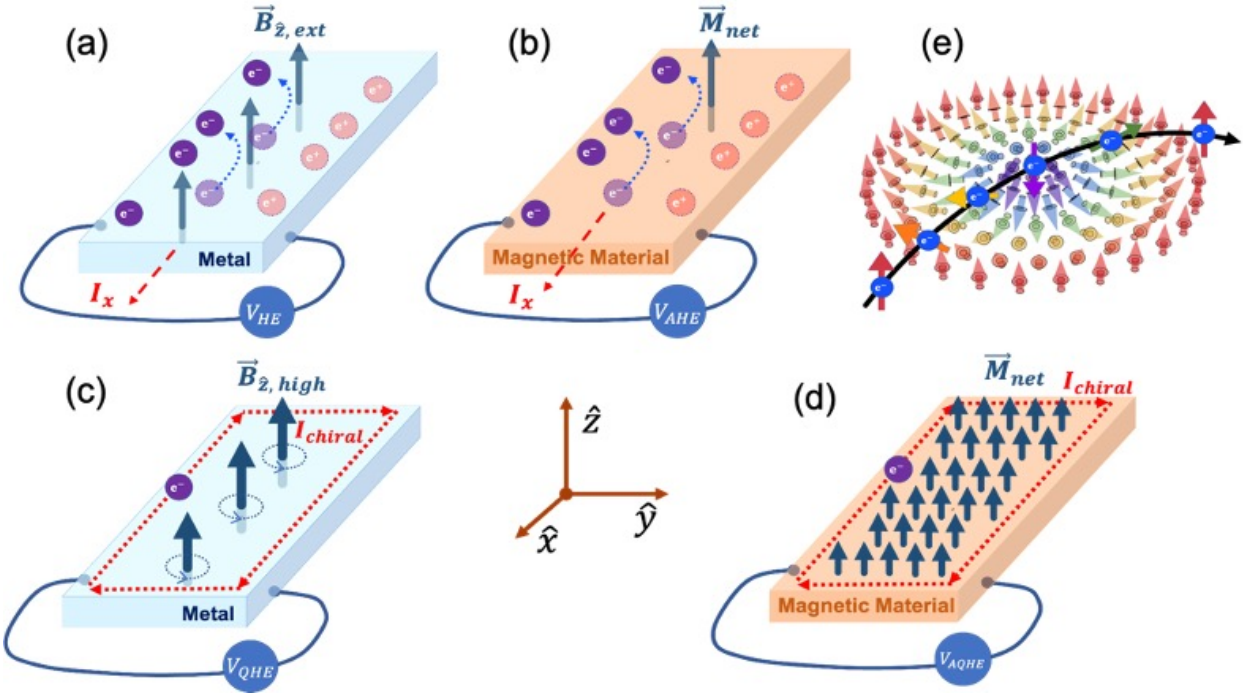

Figure 3.3.1: Family of Hall effects. (a) Charge Hall effect. (b) Anomalous charge Hall effect due to net magnetization in the magnetic material. (c) Quantum Hall effect. And (d) Anomalous Quantum Hall effect due to the strong net magnetic moments. (e) Topological Hall effect, arising due to the topological aspects of the material. Here the THE shown is due to the Skyrmion.

3.3.1 Kubo formula

The Kubo formula of Hall conductivity can be derived and interpreted in many ways. It can be derived using the Linear response formalism for QAHE from the semiclassical Boltzmann equation, or using the Kubo formalism for QAHE. Ultimately we obtain a similar kind of formula for Hall conductivity[12]. Here we derive derive this formula for any general Hall effect irrespective of its origin. We do it by considering a first order non degenerate perturbation approximation of a 2D system of electrons gas. This system subjected to a perturbation due to a small electric field along y direction which will be due to the Hall voltage, then the perturbation hamiltonian is given by eE_y. Let $\{|\alpha\rangle\}$ be the unperturbed states. The first order perturbed state $|\alpha'\rangle$ is given by,

$$|\alpha'\rangle = |\alpha\rangle + \sum_{\beta\neq\alpha} \frac{\langle\beta|\, eE\hat{y}\,|\alpha\rangle}{E_\alpha - E_\beta}\,|\beta\rangle \tag{3.3.1}$$

Then the current density in x direction due to the perturbation is written as,

$$j_x = \frac{1}{L^2}\sum_{\alpha} f(E_\alpha)\,\langle\alpha'|\,\hat{j}_x\,|\alpha'\rangle \tag{3.3.2}$$

$$= \frac{1}{L^2}\sum_{\alpha} f(E_\alpha)\left[\sum_{\beta\neq\alpha}\frac{\langle\alpha|\left(-e\hat{v}_x\right)|\beta\rangle\langle\beta|\, eE_y\hat{y}\,|\alpha\rangle}{E_\alpha - E_\beta}\,|\beta\rangle\right] + c.c. \tag{3.3.3}$$

where, $f(E_\alpha)$ is the Fermi-Dirac distribution, L^2 is the area of the magnetic unit cell. Since the perturbation is an odd function, there is no first order correction to the energies, $E_{\alpha'} = E_\alpha$.

$$\langle\beta|\,\hat{v_y}\,|\alpha\rangle = \langle\beta|\,\hat{\dot{y}}\,|\alpha\rangle \tag{3.3.4}$$

$$= \frac{-i}{\hbar}\langle\beta|\left[\hat{y},\hat{\mathcal{H}}\right]|\alpha\rangle \tag{3.3.5}$$

$$= \frac{-i}{\hbar}(E_\alpha - E_\beta)\langle\beta|\,\hat{y}\,|\alpha\rangle \tag{3.3.6}$$

substituting in the above equation 3.3.3, and plugging it in the transverse conductivity defined as the ratio of Transverse current density to (j_x) to Hall electric field (E_y) we get the Kubo formula,

$$\sigma_{xy} = \frac{j_x}{E_y} = \frac{e^2\hbar}{iL^2}\sum_{\alpha} f(E_\alpha)\left[\sum_{\beta\neq\alpha}\frac{\langle\alpha|\,\hat{v}_x\,|\beta\rangle\langle\beta|\,\hat{v}_y\,|\alpha\rangle - \langle\alpha|\,\hat{v}_y\,|\beta\rangle\langle\beta|\,\hat{v}_x\,|\alpha\rangle}{(E_\alpha - E_\beta)^2}\right] \tag{3.3.7}$$

In the next section it will become evident that the Hall conductivity is related topology of the system via the sum of the Berry curvature over the entire magnetic unit cell.

3.3.2 TKNN relation

[5] Schrodinger equation for the bloch electron in magnetic field in the reciprocal space becomes,

$$\hat{\mathcal{H}}_{\vec{k}}U_{\vec{k},n}(\vec{r}) = E_{\vec{k},n}(\vec{r})U_{\vec{k},n}(\vec{r}) \tag{3.3.8}$$

Let us consider the magnetic Bloch wavefunction in Dirac notation is $\left|n,\vec{k}\right\rangle$, then,

$$\left\langle n,\vec{k}\right|\vec{v}\left|m,\vec{k'}\right\rangle = \delta_{\vec{k}\vec{k'}}\iint_S U^*_{\vec{k},n}\vec{v}U_{\vec{k'},m} \equiv \delta_{\vec{k}\vec{k'}}\langle n|m\rangle \tag{3.3.9}$$

Because of periodicity in reciprocal space, the integration is over the magnetic unit cell. In the reciprocal space wavefunction, the matrix elements in the Nakano-Kubo formula can be written as,

$$\langle n|\,\hat{v}_x\,|m\rangle = \frac{1}{\hbar}\langle n|\,\frac{\partial\hat{\mathcal{H}}_{\vec{k}}}{\partial k_x}\,|m\rangle \tag{3.3.10}$$

$$\langle n|\,\hat{v}_y\,|m\rangle = \frac{1}{\hbar}\langle n|\,\frac{\partial\hat{\mathcal{H}}_{\vec{k}}}{\partial k_y}\,|m\rangle \tag{3.3.11}$$

Now, using the above in Nakano-Kubo formula for Hall conductivity 3.3.7.

$$\sigma_{xy} = -\frac{ie^2}{L^2}\sum_{\vec{k}}\sum_{n} f(E_{\vec{k},n})\left[\sum_{m\neq n}\frac{\left\langle m,\vec{k}\right|\frac{\partial\hat{\mathcal{H}}_{\vec{k}}}{\partial k_x}\left|n,\vec{k}\right\rangle\left\langle n,\vec{k}\right|\frac{\partial\hat{\mathcal{H}}_{\vec{k}}}{\partial k_y}\left|m,\vec{k}\right\rangle}{(E_{m,\vec{k}}-E_{n,\vec{k}})^2}\right] + c.c. \tag{3.3.12}$$

$$\langle n|\ \frac{\partial\hat{\mathcal{H}}_{\vec{k}}}{\partial k_j}\ |m\rangle = (E_m - E_n)\left\langle n\middle|\frac{\partial U_m}{\partial k_j}\right\rangle \tag{3.3.13}$$

$$= -(E_m - E_n)\left\langle \frac{\partial U_n}{\partial k_j}\middle| m\right\rangle, \quad j = x, y \tag{3.3.14}$$

Now substituting this in equation 3.3.12, we will get,

$$\sigma_{xy} = -\frac{ie^2}{L^2}\sum_{\vec{k}}\sum_{n} f(E_{\vec{k},n})\sum_{m\neq n}\left[\left\langle\frac{\partial U_n}{\partial k_x}\middle|m\right\rangle\left\langle m\middle|\frac{\partial U_m}{\partial k_y}\right\rangle - \left\langle\frac{\partial U_n}{\partial k_y}\middle|m\right\rangle\left\langle m\middle|\frac{\partial U_m}{\partial k_x}\right\rangle\right] \tag{3.3.15}$$

$$= -\frac{ie^2}{L^2}\sum_{\vec{k}}\sum_{n} f(E_{\vec{k},n})\left[\left\langle\frac{\partial U_n}{\partial k_x}\middle|\frac{\partial U_n}{\partial k_y}\right\rangle - \left\langle\frac{\partial U_n}{\partial k_y}\middle|\frac{\partial U_n}{\partial k_x}\right\rangle\right] \tag{3.3.16}$$

Let $\vec{A}_{n,\vec{k}}$ be a vector field as defined below,

$$\vec{A}_{n,\vec{k}} = \int U^*_{n,\vec{k}}\nabla_{\vec{k}}U_{n,\vec{k}}d^2r = \left\langle U_{n,\vec{k}}\right|\nabla_{\vec{k}}\left|U_{n,\vec{k}}\right\rangle \tag{3.3.17}$$

Since $\nabla_{\vec{k}}$ has the components as $\frac{\partial}{\partial k_1}$ and $\frac{\partial}{\partial k_2}$. Let E_f be the Fermi energy and rewriting the equation of Hall conductivity in terms of integral over the magnetic Brillouin zone (MBZ) we get,

$$\sigma_{xy} = \frac{e^2}{h}\frac{1}{2\pi i}\sum_{E\leq E_f}\iint_{MBZ} d^2k\left[\nabla_{\vec{k}}\times\vec{A}_{n,\vec{k}}\right]_z \tag{3.3.18}$$

Because the edges of the MBZ form a 2D Torus (T^2), topologically rather than a simple rectangle in the reciprocal space. Since torus does not have a boundary, the above integral is zero for the uniquely defined values of $\vec{A}_{n,\vec{k}}$ within this torus (T^2). Then σ_{xy} gets a non zero contribution when $\vec{A}_{n,\vec{k}}$ has non trivial topology. To understand the effect of topology on $\vec{A}_{n,\vec{k}}$, we shall consider a local guage transformation, where the $\vec{k}$-space wavefunction is transformed continuously by any arbitrary continuous function $f(\vec{k})$,

$$U_{n,\vec{k}}(\vec{r}) \longrightarrow U'_{n,\vec{k}}(\vec{r}) = e^{if(\vec{k})}U_{n,\vec{k}}(\vec{r}) \tag{3.3.19}$$

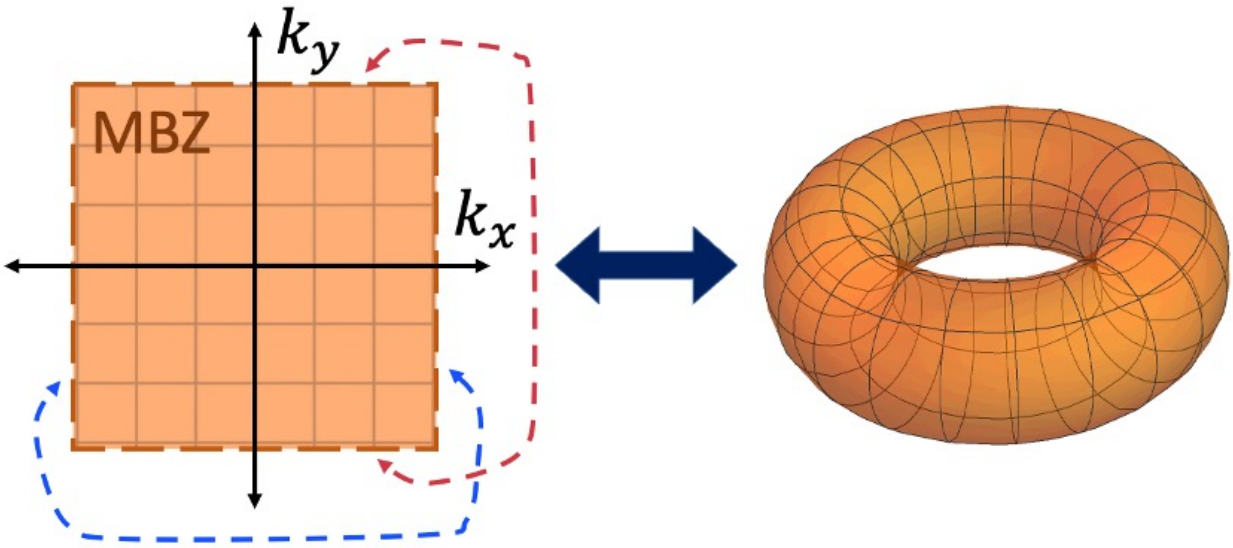

Figure 3.3.2: Equivalence in topology of a Magnetic brillouin zone and torus.

Substituting this in the definition of $\vec{A}_{n,\vec{k}}$ in equation 3.3.17 we get,

$$\vec{A'}_{n,\vec{k}} = \vec{A}_{n,\vec{k}} + i\nabla_{\vec{k}} f(\vec{k}) \tag{3.3.20}$$

From equation 3.3.18 and the above transformation equation, it becomes evident that σ_{xy} is proportional to the sum of the chern numbers defined in equation 2.2.17. So for topologically non trivial system. The total transverse conductivity between two bands in the bandgap is integer quantised and is given by the famous TKNN relation,

$$\sigma_{xy} = \frac{e^2}{h} \sum_n C_n \tag{3.3.21}$$

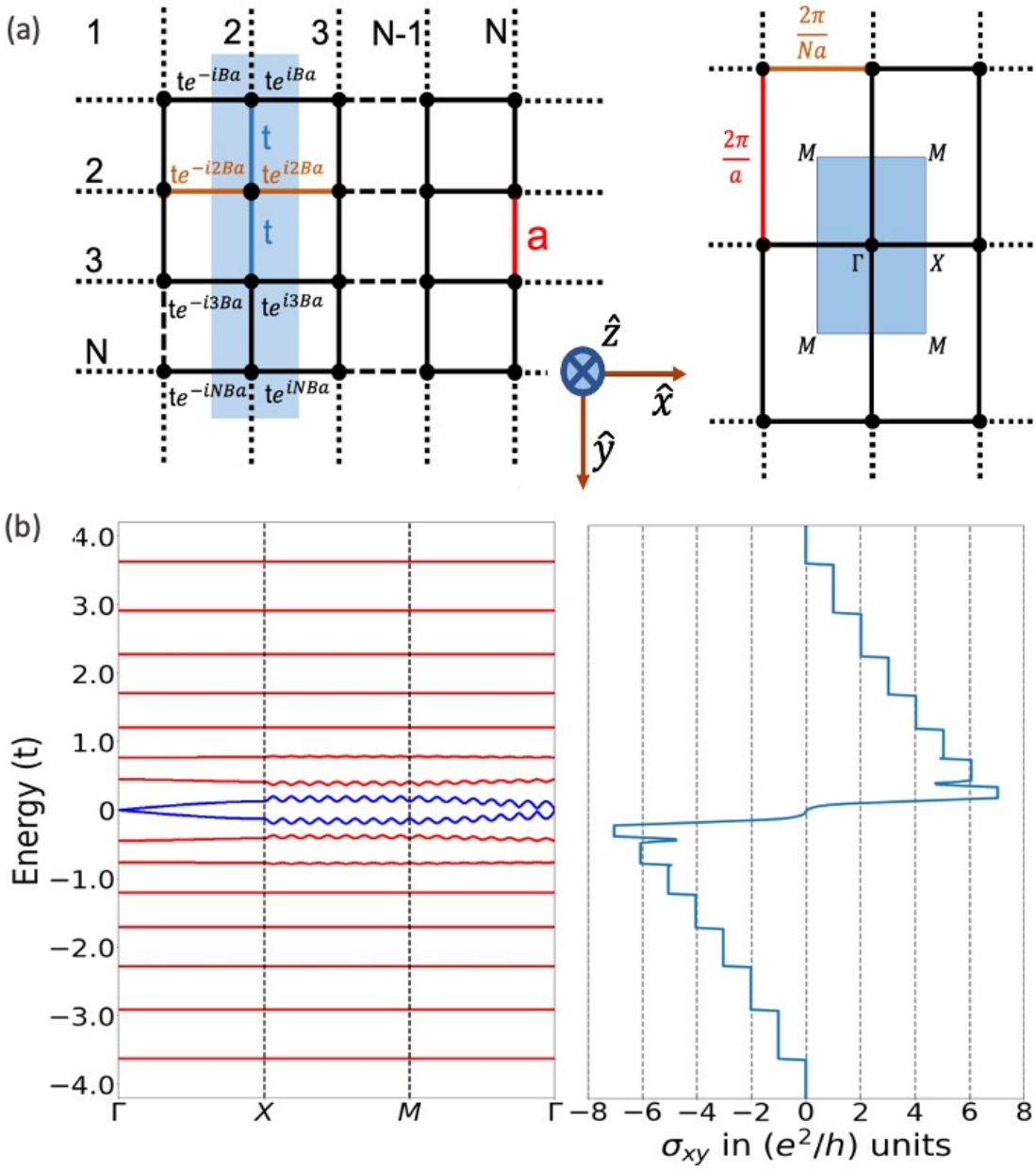

Figure 3.3.3: IQHE on a square lattice, calculated within the tight-binding framework. Panel (a) shows the magnetic unit cell and the magnetic brillouin zone for the generalised case on a square lattice. Landau guage is assumed ($\vec{A} = (0, Bx, 0)$ and $\vec{B} = (0, 0, B)$). Magnetic flux per unit cell is taken to be 1. Panel (b) is the electronic band structure for a 16 site unit cell (N = 16, a = 1, t = 1). The bands in red have a Chern number -1 and the blue bands have Chern number +7. The last panel shows the quantised transverse hall conductance with plateaus at the band gaps as explained by the TKNN relation.

Chapter 4

Eletron Transport in a Skyrmion Crystal

In this chapter, we discuss the transport of an itinerant electron in a Skyrmion crystal state. This problem is addressed from the framework of tight-binding approximation. The itinerant electron experiences a topological magnetic field whose effect is given by the berry curvature in the reciprocal space. In the first section we establish this effect of topological magnetic field in the tight-model and diagonalize it into an effective tight-binding model of a IQHE hamiltonian in the infinite Hund's coupling limit.

4.1 Tight - Binding description

We begin with a free-electron system interacting with the background spin texture $\vec{n}_i$ via Hund's coupling mechanism.[13] Then Hamiltonian is given by the double exchange model as,

$$\hat{\mathcal{H}} = \sum_{<ij>} t_{ij}\hat{c}_i^\dagger \hat{c}_j - J\sum \hat{c}_i^\dagger(\vec{n}_i.\vec{\sigma})\hat{c}_i \tag{4.1.1}$$

here, the $\hat{c}_i^\dagger$ is the two component (spin up and spin down) creation operator at the site i. Similarly $\hat{c}_i$ is the two component annhilation operator at the site i. t_{ij} is the transfer integral between nearest-neighbor sites, J is the Hund's coupling strength between the electron spin and the background spin texture. And $\vec{\sigma}$ denotes the Pauli matrices. In the strong Hund's coupling limit, $(J \gg t_{ij})$, the spin of the hopping electron is forced to align parallel to the spin texture.

So we are diagonalizing the Hund's coupling term to always be in spin up direction. This transformation change the refence from the global frame of reference of the entire crystal to the local reference frame of the moving electron. The transformation is given by,

$$\hat{U}_i^\dagger(\vec{n}_i.\vec{\sigma})\hat{U}_i = \sigma_z \tag{4.1.2}$$

here $\hat{U}_i$ is the unitary transformation matrix relating the annhilation (creation) operators in the global and local basis as,

$$\hat{C}_i = \hat{U}_i \hat{d}_i \tag{4.1.3}$$

$$\hat{C}_i^\dagger = \hat{d}_i^\dagger \hat{U}_i^\dagger \tag{4.1.4}$$

also the Unitary transformation operator is given by,

$$\hat{U}_i = \begin{bmatrix} \cos\left(\frac{\theta_i}{2}\right) & e^{-i\phi_i}\sin\left(\frac{\theta_i}{2}\right) \\ e^{i\phi_i}\sin\left(\frac{\theta_i}{2}\right) & \cos\left(\frac{\theta_i}{2}\right) \end{bmatrix} \tag{4.1.5}$$

Here the columns representing the eigen vectors ($\left|\chi_i^\uparrow\right\rangle$ and $\left|\chi_i^\downarrow\right\rangle$) of the hunds coupling term with eigenvalues 1 and -1 respectively. In this new basis, the Hamiltonian becomes,

$$\hat{\mathcal{H}} = \sum_{<ij>} t_{ij} \hat{d}_i^\dagger \hat{U}_i^\dagger \hat{U}_j \hat{d}_j - J \sum \hat{d}_i^\dagger \hat{U}_i^\dagger (\vec{n}_i.\vec{\sigma}) \hat{U}_i \hat{d}_i \tag{4.1.6}$$

$$= \sum_{<ij>} t_{ij} \hat{d}_i^\dagger \hat{U}_i^\dagger \hat{U}_j \hat{d}_j - J \sum \hat{d}_i^\dagger \sigma_z \hat{d}_i \tag{4.1.7}$$

Then the effective hopping is given by,

$$t_{ij}^{eff} = t_{ij} \hat{U}_i^\dagger \hat{U}_j \tag{4.1.8}$$

which is given by,

$$\hat{U}_i^\dagger \hat{U}_j = \begin{bmatrix} \cos\left(\frac{\theta_i}{2}\right)\cos\left(\frac{\theta_j}{2}\right) + \sin\left(\frac{\theta_i}{2}\right)\sin\left(\frac{\theta_j}{2}\right)e^{-i(\phi_i-\phi_j)} & -e^{i\phi_i}\sin\left(\frac{\theta_i}{2}\right)\cos\left(\frac{\theta_j}{2}\right) + e^{-i\phi_j}\cos\left(\frac{\theta_i}{2}\right)\sin\left(\frac{\theta_j}{2}\right) \\ e^{-i\phi_i}\sin\left(\frac{\theta_i}{2}\right)\cos\left(\frac{\theta_j}{2}\right) + e^{i\phi_j}\cos\left(\frac{\theta_i}{2}\right)\sin\left(\frac{\theta_j}{2}\right) & \cos\left(\frac{\theta_i}{2}\right)\cos\left(\frac{\theta_j}{2}\right) + \sin\left(\frac{\theta_i}{2}\right)\sin\left(\frac{\theta_j}{2}\right)e^{i(\phi_i-\phi_j)} \end{bmatrix} \tag{4.1.9}$$

$$= \begin{bmatrix} \left\langle \chi_i^\uparrow \middle| \chi_j^\uparrow \right\rangle & \left\langle \chi_i^\uparrow \middle| \chi_j^\downarrow \right\rangle \\ \left\langle \chi_i^\downarrow \middle| \chi_j^\uparrow \right\rangle & \left\langle \chi_i^\downarrow \middle| \chi_j^\downarrow \right\rangle \end{bmatrix} \tag{4.1.10}$$

For the strong-coupling limit only the component that is parallel to the spin up direction contribute,

and the parallel to spin down direction becomes more energetically costly,

$$t_{ij}^{eff} = t_{ij} \left\langle \chi_i^{\uparrow} \middle| \chi_j^{\uparrow} \right\rangle \tag{4.1.11}$$

$$= t_{ij} \left(\cos\left(\frac{\theta_i}{2}\right) \cos\left(\frac{\theta_j}{2}\right) + \sin\left(\frac{\theta_i}{2}\right) \sin\left(\frac{\theta_j}{2}\right) e^{-i(\phi_i - \phi_j)} \right) \tag{4.1.12}$$

The diagonalized Hund's coupling term in the Hamiltonian now becomes a constant for the blocks. Hence they do not change the physics but only cause and shift in overall energy. Now rewritting the effecting hopping parameter in polar form,

$$t_{ij}^{eff} = t_{ij} e^{i a_{ij}} \cos\left(\frac{\theta_{ij}}{2}\right) \tag{4.1.13}$$

where, a_{ij} is the berry phase change due to hopping of electron from site i to site j. Then a_{ij} and $\cos(\theta_{ij})$ is given by,

$$a_{ij} = \arctan\left(\frac{-\sin(\phi_i - \phi_j)}{\cos(\phi_i - \phi_j) + \cot\left(\frac{\theta_i}{2}\right) \cot\left(\frac{\theta_j}{2}\right)} \right) \tag{4.1.14}$$

$$\cos(\theta_{ij}) = \cos(\theta_i) \cos(\theta_j) + \sin(\theta_i) \sin(\theta_j) \cos(\phi_i - \phi_j) \tag{4.1.15}$$

As is well known from the book by Feynman, when an electron moves in a magnetic field, it acquires a phase factor modifying the hopping parameter to become,

$$t_{\vec{A} \neq 0} = t_{\vec{A} \neq 0} \exp\left\{ \frac{ie}{\hbar} \int_i^j \vec{A}.d\vec{r} \right\} \tag{4.1.16}$$

So, it becomes evident that in strong coupling limit, equation 4.1.13 has the above form. It means even though no external magnetic field is present, the adiabatic motion of the electron coupled to the background spin texture is equivalent to a magnetic field. This is due to the non trivial topology. Then the effective hamiltonian is given as,

$$\hat{\mathcal{H}}_{eff} = \sum_{<ij>} t_{ij} \left\langle \chi_i^{\uparrow} \middle| \chi_j^{\uparrow} \right\rangle \hat{d}_i^{\dagger} \hat{d}_j$$

4.2 Rashba and Dresselahaus Spin orbit coupling

In materials without a center of inversion either in their unit cell (bulk) or at their surface, the spin-orbit coupling induces a unique form of Zeeman interaction in momentum space; the electron's spin is locked on an effective magnetic field that is odd in momentum. The resulting inter play between the electron's momentum and its spin promotes a wealth of physical mechanisms that

have attracted extraordinary attention through many decades.[14]

A pedagogical approach to the microscopic origin of Rashba spin orbit coupling states that the potential gradient at an interface is dominated by the electric field normal to this interface, otherwise, this interfacial potential gradient does not impact the spin-orbit coupling itself, but rather the Bloch wave function of the conduction electrons such that they acquire a momentum dependent orbital moment. The key feature of Rashba spin-orbit coupling is the linear coupling between the carrier's spin angular momentum and its linear momentum k. In other words, the electron's spin and linear momenta are locked with each other. The mathematical form of Rashba spin-orbit coupling at interfaces is given,

$$\hat{\mathcal{H}}_R = \lambda_R \vec{\sigma}.(\hat{z} \times \vec{k}) \tag{4.2.1}$$

here, α_R is the Rashba interaction strength. and $\vec{\sigma}$ is the usual Pauli spin matrices. In the second quantised form this hamiltonian can be expressed in terms of the two particle creation ($\hat{c}^\dagger$) and anhiliation ($\hat{c}$) operators as,

$$\hat{\mathcal{H}}_R = -i\lambda_R \sum_{<ij>} \hat{c}_i^\dagger \vec{\sigma}.(\hat{z} \times \vec{r}_{ij})\hat{c}_j \tag{4.2.2}$$

$$= -i\lambda_R \sum_{<ij>} \hat{c}_i^\dagger (\sigma_x r_y - \sigma_y r_x)\hat{c}_j \tag{4.2.3}$$

A similar spin orbit interaction that arises due to the broken inversion symmetry in the bulk is called the Dresselhaus spin orbit coupling[15]. In reciprocal space it is given by,

$$\hat{\mathcal{H}}_D = -i\lambda_D \sum_{<ij>} \hat{c}_i^\dagger (\sigma_x r_x - \sigma_y r_y)\hat{c}_j \tag{4.2.4}$$

The influence of these SOC on the THE on SkX is analysed in the next chapter.

Chapter 5

Results & Analysis

In this section the results obtained using the numerical computation on a honeycomb lattice are listed and are explained in detail using the Onsager's quantization scheme. Initially the hamiltonian with Hund's coupling term in the finite coupling limit is studied then the large Hund's coupling limit case is studied. Later, the models with added Rashba and Dresselhaus spin orbit coupling are analysed.

The Topological Hall Effect in a Skyrmion crystal is closely related to the Integer QHE. And the one-to-one correspondence between them has been established in the previous chapter. This correspondance in the bands and the Chern numbers are true except at energies close to Van Hove Singularity energy of the zero effective magnetic field case. Even in this region the Hall conductivities of are similar to each other in case of large skyrmions. The THE in SkXs is quantized, as like in the QHE.

The magnetic texture of a skyrmion carries an integer topological charge (± 1 for skyrmion and anti-skyrmion respectively). This gives rise to an emergent effective magnetic field that is collinear with a nonzero average. Hence the Hall conductivity of the THE is similar to the conductivity of the QHE with a corresponding homogeneous magnetic field with $p/q = W_{Sk}/n = \pm 1/n$, here n is the number of atoms in the skyrmion unit cell. The main difference between the THE and QHE is the inhomogeneity of the emergent field (THE has inhomogeneous emergent field; QHE: homogeneous applied field). This inhomogeneity is reason for the deviation from the almost flat LLs of the QHE and redistribution of their Berry curvature. But near a VHS, the LLs are so close to each other that this deviation is more and could alter the Chern numbers and, thus, the conductivity.[16]

Landau Levels, Hall Conductivity

The band structure for $B_{eff} = 0$ (i.e., the zero-field band structure, depicted within the structural Brillouin zone in panel (a) of figure below) has amaximum at E = +3 t , aminimum at E = -3 t and

two VHSs at $E_{VHS} = \pm 1$ (for t = 1 case). The Dirac point is observed at $E_{DP} = 0$. For $B_{eff} > 0$, the band structure in large coupling limit are symmetrically distributed about the DP. Only the bands near the VHS shows large oscillations. At the otherhand, LLs close to the band edges shoes least oscillations. The positions of maxima and minima of every alternating bands coincide.

For J = 0t, the spin is not coupled to the skyrmion texture and the bands are spin-degenerate. The band structure of the honeycomb lattice is back-folded into the magnetic Brillouin zone. The bands appear between $E = \pm 3t$ with a bandwidth of 6t ; 2 VHSs and a DP appear respectively at $E_{VHS} = \pm 1t$ and $E_{DP} = \pm 0t$.

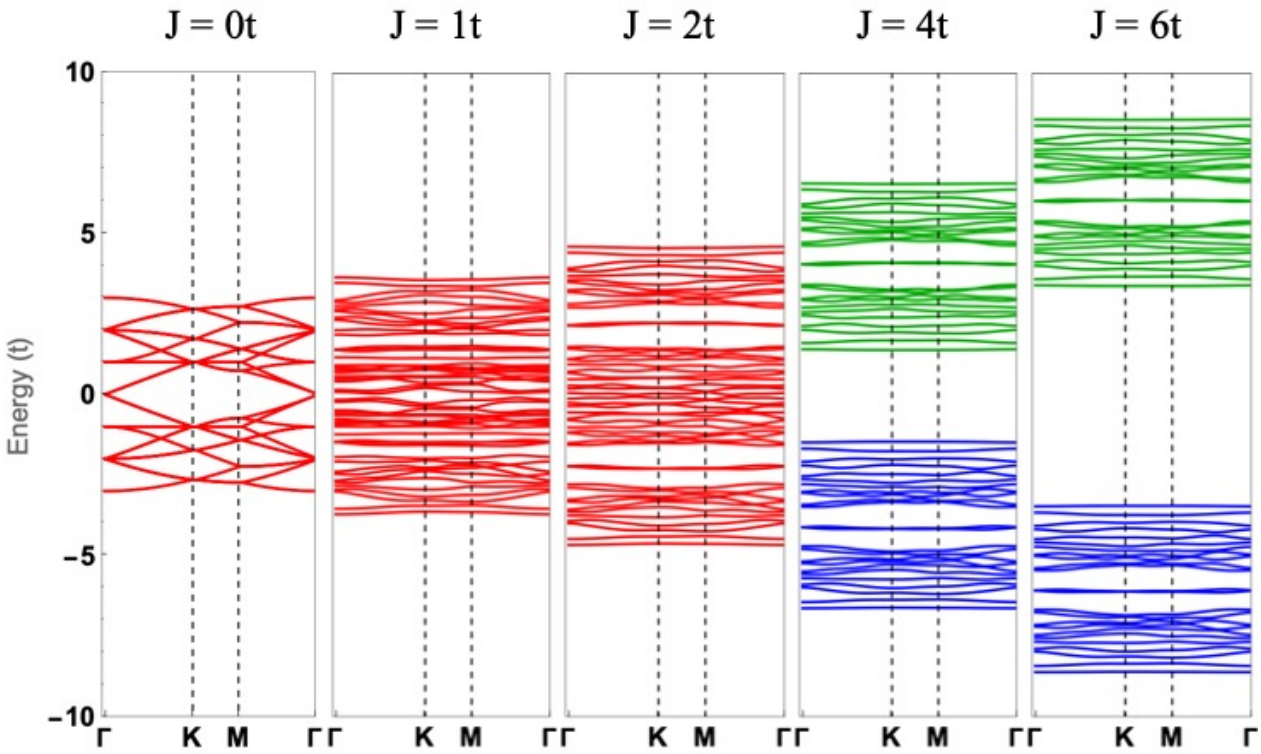

Figure 5.0.1: Band structure for the model with finite Hund's coupling. The skyrmion unit cell contains 24 sites from the honeycomb lattice. The skyrmion considered has $W_{sk} = +1$. The total number of bands obtained from this model is 48. Blue colour represents bands with parallel alignment of itinerant electron with the skyrmion spin texture. Green colour represents the antiparallel alignment of the same.

For non zero J, the spins align with the skyrmion texture and the bands are no more spin degenerate (J = 1t & 2t from figure 5.0.1). Increasing J further, the bands are separated into two blocks: one with spins parallel, the other with spins anti-parallel to the skyrmion texture (blue and green coloured bands form figure 5.0.1). While for J = 6 t both blocks deviate in details, in the limit ($J \gg t$) both blocks exhibit rigidly shifted dispersion relations. The band blocks, with width

is also 6t and are shifted by $\pm J$.While the edge bands of each block are well separated and quite less dispersive, around the VHSs the bandwidths and gaps are considerably smaller.

The band structures are invariant with respect to changes of the skyrmion helicity. While continuously turning a Néel into a Bloch-type skyrmion and the skyrmion charge. For strong coupling, the electron spins are fully aligned parallel with the skyrmion texture. Thus, it is sufficient to consider only one band block, which then describes spinless electrons. This was shown in the previous chapter.

In the large coupling limit, the transverse Hall conductivity σ_{xy} as a function of the fermi energy is zero at energies below (above) the band bottom (top) E = -3t (+3t) of the zero field band structure. With increasing energy, σ_{xy} decreases in steps of $\sigma_o = e^2/h$ at each LL. This is readily explained by their Chern numbers of -1 and the TKNN relation. These steps comply with LLs of free electrons and are abrupt because the associated LLs are practically dispersion less. Between the two VHSs the Hall conductivity is unconventionally quantised in steps of $2\sigma_o$. The hall conductivity is anti-symmetric about the DP with in the same spin block. this reflects the symmetric shape of the zero-field band structure. The considerably large oscillation amplitudes of the LLs near the VHS manifest themselves as modulations in the Hall conductivity. This is explained by the Berry curvature which is non uniformly distributed within the Brillouin zone, in contrast to the Berry curvature of free-electron LLs. However, the Chern numbers will be -1.

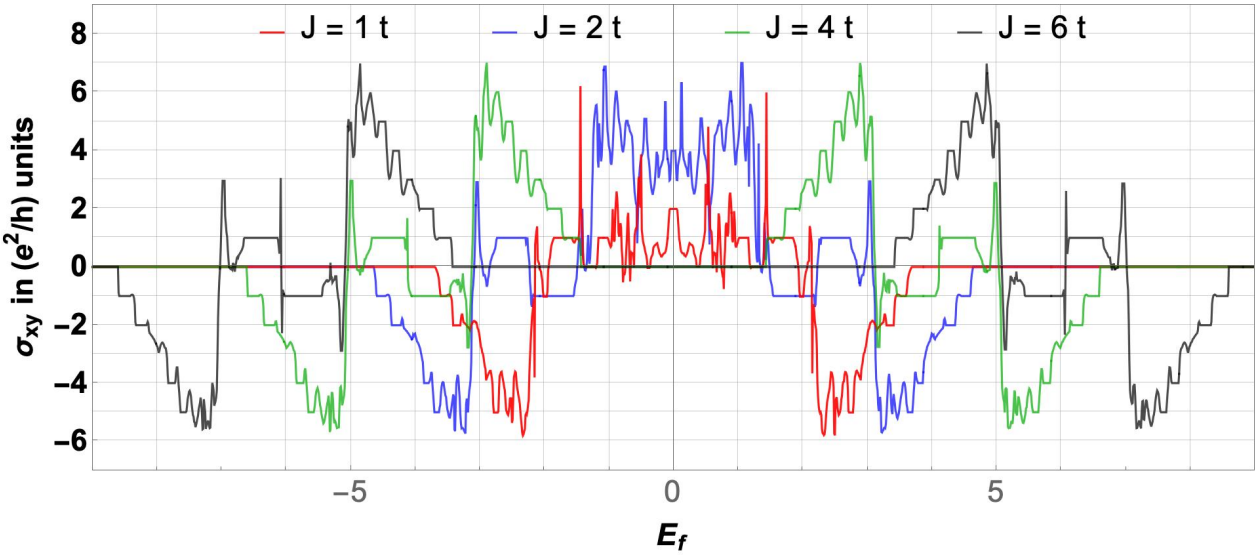

Figure 5.0.2: Quantised Hall conductivity for diffrent coupling strengths shown in figure 5.0.1. For $J \leq 2t$ the blocks of bands are not well separated according to the spin alignment of electron. There is quantization in this regime but it is not so prominent. When $J < 2t$ the spin blocks become separate. So the resonably large coupling approximation for this system $J > 3t$

.

Fermion character

To explain the above findings it can be assumed that the LLs can be separated into more free-electron type levels and lattice influenced ones. LLs of the first type have the least dispersion and are situated at the band edges, possess an almost constant Berry curvature with chern number -1. The second type shows at energies close to VHS, with oscillations in both energy and Berry curvature; the positions (in reciprocal space) of their extrema coincide with those of their Berry curvature.

Now, we discuss the Berry curvature distributions in detail. For this purpose we determine the fermion character of the electrons at constant-energy cuts of the zero-field band structure. At low energies (panel vii in figure 5.0.3) the dispersion is almost parabolic and the circular Fermi line encloses occupied states. This electron pocket has positive curvature and is associated with a positive effective mass ($m^* > 0$).

With increasing energy, the dispersion deviates more and more from that of free electrons; the constant energy contours become warped but the Fermi lines remain electron like. At lower VHS (panel vi in figure) the Fermi line is a hexagon resembling the lattice geometry; its vanishing berry curvature implies an infinite effective mass. Hence, the Lorentz force of an external magnetic field leaves the electronic states unaffected, which explains why the LLs close to EVHS show oscillations that resemble the zero-field band structure.

At even higher energy that lies between the lower VHS and the DP. There are now 2 hole pockets with negative curvature in band structure hence having a negative effective mass. But the dispersion again becomes parabolic when it is away from the VHS till the DP. At DP the there is no electron or hole pocket. Above the DP level, the zero field band is symmetric with respect to the DP level, So the same explanation applies there too but with the electron and hole pockets interchanged.

The Berry curvature of a band is dominated by contributions from the adjacent bands. The maxima of band n coincide with the minima of the adjacent band above, its minima coincide with the maxima of the adjacent band below. The fermion character defines the sign of Berry curvature. This is in agreement with the numerical results: below (above) the VHS, i.e., in the electron (hole) regime with $m^* > 0$ ($m^* < 0$), energy maxima coincide with minima (maxima) of the Berry curvature. As a result, the Berry curvature contributions of the maxima and minima of the LL oscillations cancel out and the Chern number of -1 is that of free-electron LLs. The above reasoning does not hold for the LL near the VHS because its Berry curvature is dictated by states below and above the VHS. Therefore, the dispersion minima are electron like, which leads to a maximum of the Berry curvature. The maxima are hole like and, thus, also coincide with maxima of the Berry curvature, overall the Berry curvature of this particular LL is positive throughout.

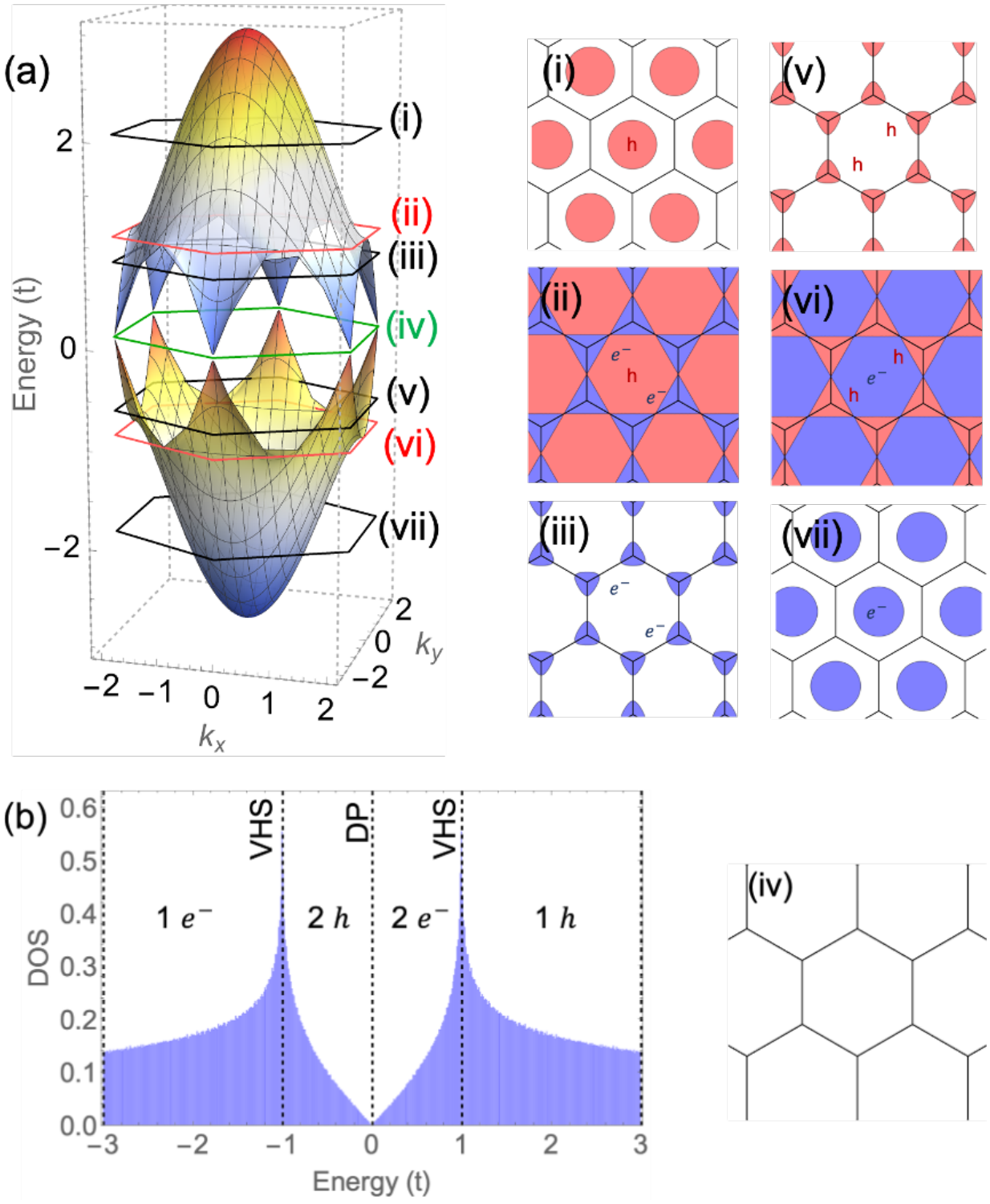

Figure 5.0.3: Onsager's Quantization Scheme. (a) Zero field bands of the honey comb lattice. Panels (i) - (vii) are the constant energy cross cross sections showing the hole (red) and electron (blue) pockets respectively. (b) shows the Density of states for the zero field bands. Panel (iv) is the cross section at the Dirac point energy. It has no hole or electron pocket. But there is a hole pocket below and electron pocket above the Dirac point. This explains the change in sign of Hall conductivity at the Dirac point. Image inspiration [16][17]

Unconventional Quantization

If a Fermi line encloses an area $\xi = n(j + 1/2)\xi_o$, here n is the number of hole or electron pockets in the zero field band, j is an integer, $\xi_o = F/q$, F area of the Brillouin zone and q is the number of sites in the magnetic unit cell. Irrespective of the fermion character, a dispersion less LL is formed at the respective energy, according to Onsager's quantization scheme.

Size effects near VHS

The sawtooth shape of σ_{xy} becomes more pronounced when the skyrmion size becomes larger. The steps as well as the jump become energetically more narrower because there are more bands within the same energy range. Refer figure 5.0.4. At DP, Lifshitz transition happens which is accompanied by the change of the fermion character from electron to a hole or vice versa respectively. For a $+1$ charged skyrmion it changes from hole to electron.[18]

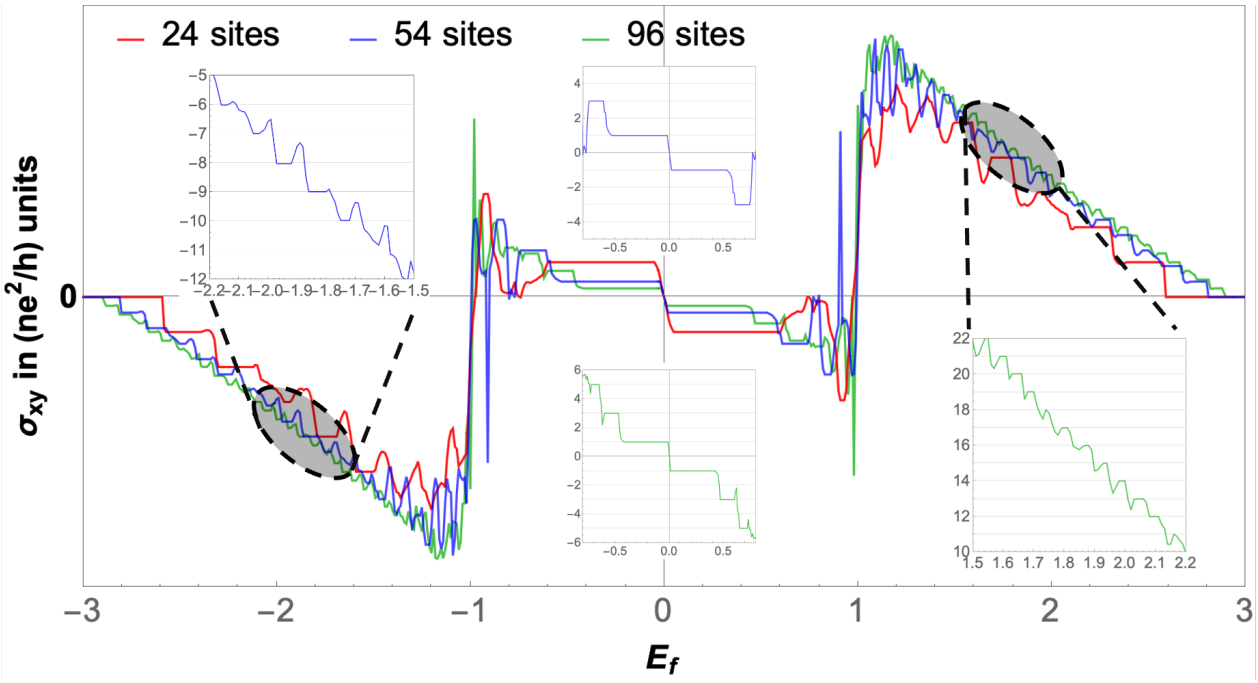

Figure 5.0.4: Size effets on the quantization. Quantised Hall conductivity for a skyrmion with charge +1 is shown for 3 different skyrmion sizes . The quantization becomes more prominent near the VHS region when the skyrmion size becomes larger. Here n is the number of sites in the skyrmion unit cell.

Large coupling limit

In the large coupling approximation, the bands and conductivity of the parallel and anti-parallel blocks are antisymmetric about the DP enenrgy level of the zero field band. Even though the bands for the spin blocks are shifted by the coupling stength they are not exactly identical. The bands away from the VHS of the both the blocks matches. But the bands near VHS are not identical for both spin blocks. But the explanations for the quantization based on the zero field bands is valid.

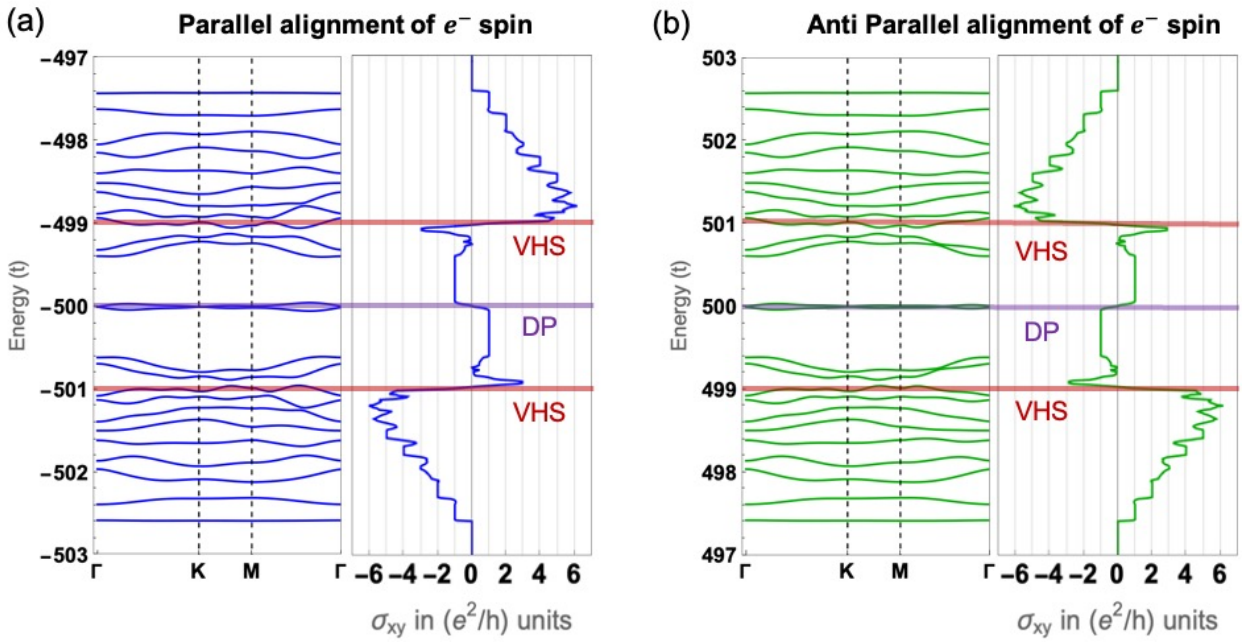

Figure 5.0.5: Large Hund's coupling limit J = 500t. (a) the band structure and the quantized hall conductivity of block of the parallel spin alignment of the itinerant electron with the surrounding spin texture. (b) anti parallel block of the same. It becomes evident that in the both blocks the bands structure and the σ_{xy} is antisymmetric about the DP level. But the blocks are not identical with eachother. This is a deviation from square lattice results.

Rashba and Dresselhaus effects on THE

When Rashba SOC discussed in previous chapter is added to the model, the hall conductivity becomes more prominent for only the Neel type skyrmion with helicity zero. This happens when the Rashba coupling strength is fine tuned. This is because the berry curvature is redistributed due to the Rashba coupling Consequently, quantization becomes more prominent. In terms of the band diagram, bands become relatively less dispersed with fine tuned Rashba coupling. Though the variation in band dispersion is not clear from the figure, it can be quantified by calculating the bandwidth for each band. As the Rashba strength is varied, at a particular value, the widths of most

bands attain their minimum value, and at this point, the conductivity exhibits the most prominent quantization. The same effect is observed for a Bloch antiskyrmion when Dresselhaus coupling is considered instead of Rashba. The conductivity is flipped in the energy range when compared with the Rashba coupling case. This is because the emergent magnetic field is proportional to the skyrmion charge, and skyrmion and antiskyrmion have a relative sign difference in their topological charge.

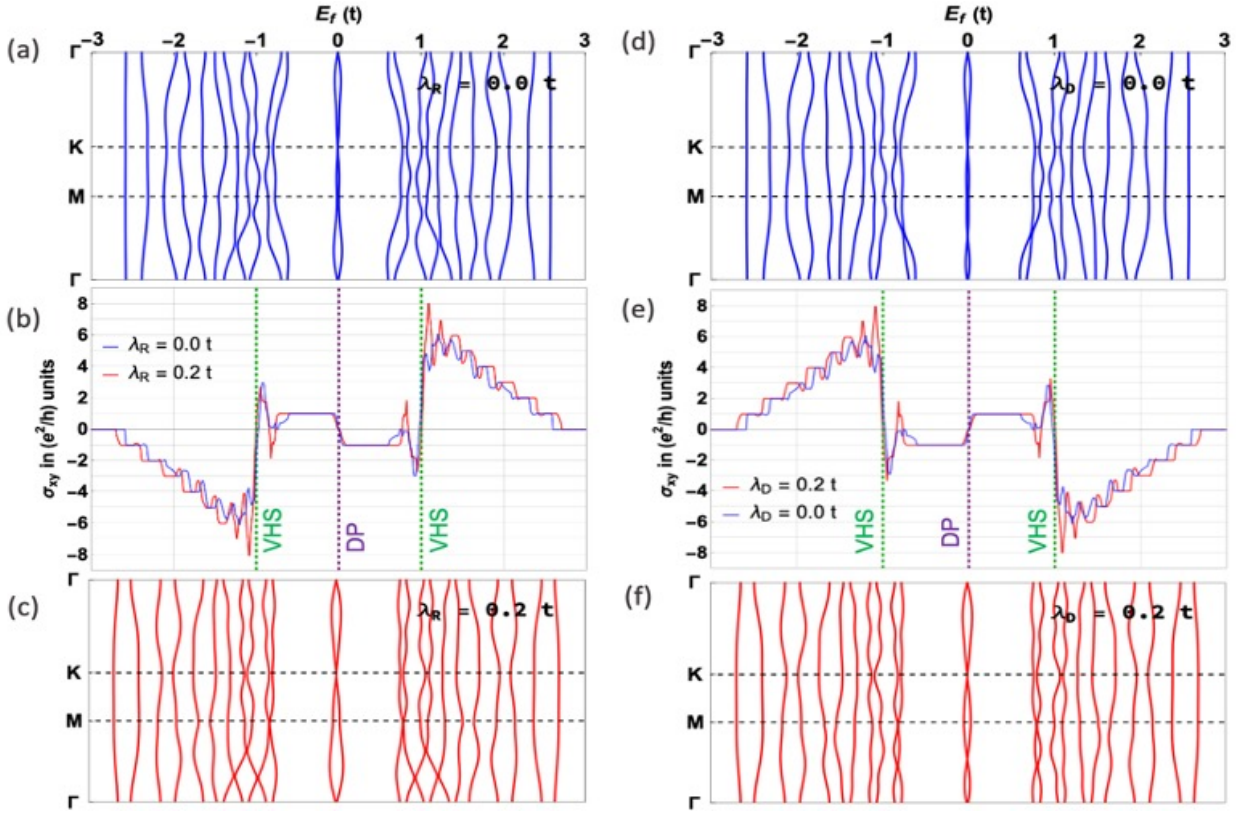

Figure 5.0.6: Rashba and Dresselhaus coupling. Panels (a) - (c), Band structure and Hall conductivity comparison without and with 0.2t Rashba coupling strength for a Neel type skyrmion. Panels (d) - (f), Band structure and Hall conductivity comparison without and with 0.2t Dresselhaus coupling strength for a Bloch type antiskyrmion.

Chapter 6

Conclusion & Future work

This study aimed at understanding the THE in honeycomb skyrmion crystal. It has been studied and linked with the IQHE. Its peculiar unconventional features were understood in terms of the zero field bands of the underlying lattice structure. The key results indicate that the Hall conductivity in the region between the van Hove singularities quantize in steps of twice the conductivity quantum $(2e^2/h)$. And in the other sides of van Hove singularities conductivity jumps in steps of $1e^2/h$. And the sign of conductivity changes at all the important points like the van Hove singularities and Dirac point. These findings suggest that the difference from the IQHE is due to the inhomogenity in the emergent magnetic fields. To homogenize the emergent magnetic field the Rashba and Dresselhaus SOC was added to the model. The main results found in this work is that the physics is same for the Rashba on Neel type skyrmions with helicity zero and Dresselhaus on Bloch antiskyrmions with helicity $-\pi/2$[19]. Though the results and analysis done at the preliminary stage due to the time constraint. It suggests that the models with SOC homogenizes the Berry curvature in the MBZ causing more prominent quantization as like in the IQHE. The code used for the numerical analysis was developed in house by myself and my collaborator Chethan with suggestions from Arijit Mandal from the lab. The code can be made available upon request. Future studies should consider on refining the results for the models with SOC and focus more on a rigorous analysis.

APPENDIX - 1

This is the python code for the IQHE in a square lattice model due to External magnetic field. Landau Guage is considered here, $\vec{A} = (0, Bx, 0)$. Hence $\vec{B} = (0, 0, B)$.

In [1]:

```
import numpy as np
import matplotlib.pyplot as plt
import pandas as pd
```

In [2]:

```
# Parameters
N = 16                # Lattice size
B = 2 * 3.14159/N       # Magnetic field
a = 1                   # Lattice constant
t = 1                   # Hopping parameter
```

In [3]:

```
" Neighbour table to impliment periodic boundary condition "
" Indexing the sites "
index = np.zeros(N)
for i in range(0, N, 1):
   index[i] = i
#print(index)

Lindex = np.zeros(N)
Rindex = np.zeros(N)
for i in range(0, N, 1):
    if i - 1 == -1 :
        left = N-1
    else :
        left = i - 1

    if i + 1 > N-1 :
        right = 0
    else :
        right = i + 1

    Lindex[i] = left
    Rindex[i] = right
#print(Lindex)
#print(Rindex)
```

In [4]:

```
" Defining the Hamiltonian Matrix "
def H(kx, ky):
    Hij = np.zeros((N,N), dtype=np.complex128)
    for i in range(0,N):
        left, right = int(Lindex[i]), int(Rindex[i])  # Convert to integers
        Hij[i][i] = 2 * t * np.cos((a*ky) + (B*a*(i+1)))
        Hij[left][i] = t * np.exp(1j * kx)
        Hij[right][i] = t * np.exp(-1j * kx)
    return Hij
```

In [14]:

```
" Band structure calculation "
# Path in the reciprocal space
GX = []
XM = []
```

```
MG = []
for i in range(0,1001):
    GX.append([0 + ( ( 3.14159 * i) / (N * 1000) ), 0])
    XM.append([3.14159/N, 0 + ( ( 3.14159 * i) / (1000) )])
for i in range(0,1001):
    point = ( 3.14159) * ((1000 - i) / (1000))
    MG.append([point/ N, point])
    point = 0

# Obtaining bands
slno  = [0]
band = np.zeros((N, len(GX) + len(XM) + len(MG)))
for i in range(0, len(GX)):
    slno.append(slno[-1]+1)
    eigen = np.sort(np.linalg.eigvalsh(H(GX[i][0], GX[i][1])))
    for b_index in range(0, N):
        band[b_index][i] = eigen[b_index]

for i in range(0, len(XM)):
    slno.append(slno[-1]+1)
    eigen = np.sort(np.linalg.eigvalsh(H(XM[i][0], XM[i][1])))
    for b_index in range(0, N):
        band[b_index][len(GX) + i] = eigen[b_index]

for i in range(0, len(MG)):
    slno.append(slno[-1]+1)
    eigen = np.sort(np.linalg.eigvalsh(H(MG[i][0], MG[i][1])))
    for b_index in range(0, N):
        band[b_index][len(GX) + len(XM) + i] = eigen[b_index]

# Remove the last element
slno = slno[:-1]
```

In [20]:

```
" full band structure plot "
f = plt.figure();
for b_index in range(0, N):
    plt.plot( slno, band[b_index], c = 'red', marker='o', linestyle='-', markersize=0
.25 )
plt.axvline(len(GX),c='k', linestyle='--', linewidth = 3)
plt.axvline(len(GX)+len(XM),c='k', linestyle='--', linewidth = 3)
plt.axvline(1,c='k', linestyle='--')
plt.axvline(len(GX)+len(XM)+len(MG),c='k', linestyle='--', linewidth = 3)
plt.ylabel("Energy (t)", fontsize=20)
plt.xlim(0, len(GX)+len(XM)+len(MG))
plt.ylim(-4.2, 4.2)
# Customize x-axis ticks with Greek symbols
plt.xticks([0, len(GX), len(GX)+len(XM), len(GX)+len(XM)+len(MG)],
           [r'$\Gamma$', r'$X$', r'$M$', r'$\Gamma$'])
```

Out[20]:

```
([<matplotlib.axis.XTick at 0x7fef40e85b80>,
  <matplotlib.axis.XTick at 0x7fef40e85bb0>,
  <matplotlib.axis.XTick at 0x7fef6371cbb0>,
  <matplotlib.axis.XTick at 0x7fef70bc27c0>],
 [Text(0, 0, '$\\Gamma$'),
  Text(1001, 0, '$X$'),
  Text(2002, 0, '$M$'),
  Text(3003, 0, '$\\Gamma$')])
```

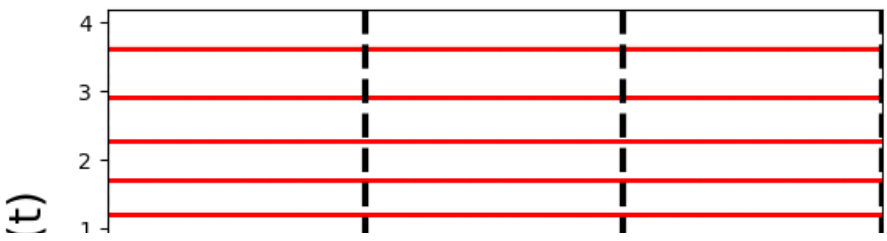

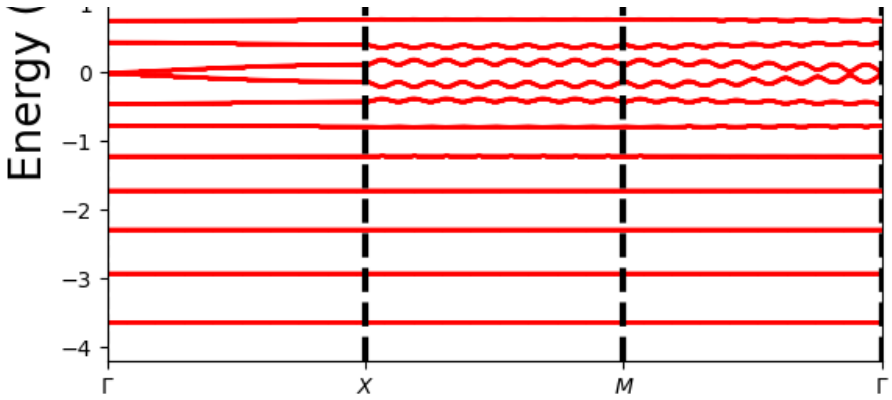

In [10]:

```
" Berry curvature calculation "
# define the derivative of the hamiltonian with respect to kx
def H_dx(kx, ky):
    Hij = np.zeros((N,N), dtype=np.complex128)
    for i in range(0, N):
        left, right = int(Lindex[i]), int(Rindex[i])  # Convert to integers
        Hij[left][i] = 1j * t * np.exp(1j * kx)
        Hij[right][i] = - 1j * t * np.exp(-1j * kx)
    return Hij

# define the derivative of the hamiltonian with respect to ky
def H_dy(kx, ky):
    Hij = np.zeros((N,N), dtype=np.complex128)
    for i in range(0,N):
        Hij[i][i] = - 2 * a * t * np.sin(a*ky + B*a*(i+1))
    return Hij

" Initializing and creating sample points in the MBZ "
grid_size = 50   # no of area elements = (grid_size)^2
kx_array = [(2 * 3.14159 * inc)/(N * grid_size) for inc in range(0, grid_size + 1)]
ky_array = [(2 * 3.14159 * inc)/(grid_size) for inc in range(0, grid_size + 1)]
#print(kx_array)
#print(ky_array)

" Some essential functions for implimenting the Berry curvature formula "
def E_value(kx, ky):
    eigenvalues = np.linalg.eigvalsh(H(kx, ky))
    return eigenvalues

def sorted_kets(kx, ky):
    eigenvalues, eigenvectors = np.linalg.eigh(H(kx,ky))
    a = np.transpose(eigenvectors)
    return a

def b_curvature(kx, ky, band_index):
    berry_curvature = 0

    band_ev = E_value(kx, ky)[band_index]
    filtered_ev = [ev for ev in E_value(kx, ky) if ev != band_ev]
    band_ket = sorted_kets(kx, ky)[band_index]
    filtered_ket = [vec for index, vec in enumerate(sorted_kets(kx, ky)) if index !=
band_index]

    dh_x = H_dx(kx, ky)
    dh_y = H_dy(kx, ky)

    for i in range(0, len(filtered_ket)):
        berry_curvature += (np.dot(np.conj(band_ket), np.dot(dh_x, filtered_ket[i]))
* np.dot(np.conj(filtered_ket[i]), np.dot(dh_y, band_ket)) - np.dot(np.conj(band_ket)
, np.dot(dh_y, filtered_ket[i])) * np.dot(np.conj(filtered_ket[i]), np.dot(dh_x, band
_ket))) / ((band_ev - filtered_ev[i] + eta)**2)
```

```
    return -berry_curvature.imag
```

In [12]:

```
" Sample Berry curvature for ground state band "
b_c_band = np.zeros((grid_size+1, grid_size+1))

for i in range(0, len(kx_array)):
    for j in range(0, len(ky_array)):
        kx = kx_array[i]
        ky = ky_array[j]
        b_c_band[i][j] = E_value(kx, ky)[4]
# Create a figure and a 3D axis
x, y = np.meshgrid(kx_array, ky_array)
fig = plt.figure()
ax = fig.add_subplot(111, projection='3d')
# Plot the data
ax.plot_surface(x, y,  b_c_band, cmap='rainbow', linewidth=0.5,rstride=5, cstride=5)
# Set labels and title
ax.set_xlabel('$k_x$',fontsize = 16)
ax.set_ylabel('$k_y$',fontsize = 16)
ax.view_init(elev=  25, azim=110)
# Show the plot
plt.show()
```

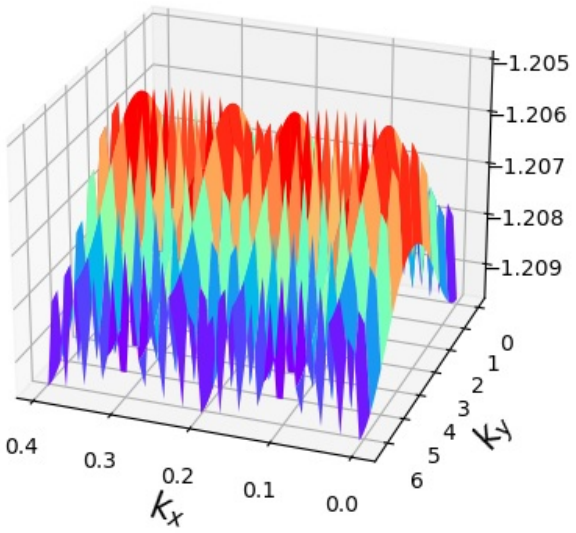

In [149]:

```
" Generating the data set in array form "
# Band data
bands = []
for band_index in range(N):
    for kx in kx_array:
        for ky in ky_array:
            bands.append(E_value(kx, ky)[band_index])
# Berry curvature data
berry_curvature = []
for band_index in range(N):
    for kx in kx_array:
        for ky in ky_array:
            berry_curvature.append(b_curvature(kx, ky, band_index))
```

In [171]:

```
" Kubo formula Implimentation "
```

```
# Parameters
Ef = [-5 + i/50 for i in range(501)]
kT = 0.00000001;

# Kubo formula part
sigma = []
for fermi_energy in Ef:
    energies = []
    bc_list = []
    for i in range(len(bands)):
        if bands[i] <= fermi_energy:
            energies.append(bands[i])
            bc_list.append(berry_curvature[i])
    if energies != []:
        conductivity = 0
        for i in range(len(energies)):
            conductivity += bc_list[i]/(1 + np.exp((energies[i] - fermi_energy)/kT))
        sigma.append(-conductivity * (1/(2*3.14 * N)) * (2 * 3.14/(grid_size))**2)
    else:
        sigma.append(0)   # Append a default value if no tuples were selected
```

In [169]:

```
" Ploting the Hall Conductivity "
f = plt.figure();
plt.plot( sigma, Ef,  marker='o', linestyle='-', markersize= 0.25 )
plt.grid()
plt.ylabel("$E_f$", fontsize=16); plt.axis('tight');
plt.xlabel("$\sigma_{xy}$ in ($e^2/h$) units", fontsize=16); plt.axis('tight');
plt.ylim(-4, 4)
plt.xlim(-8,8)
```

Out[169]:

```
(-8.0, 8.0)
```

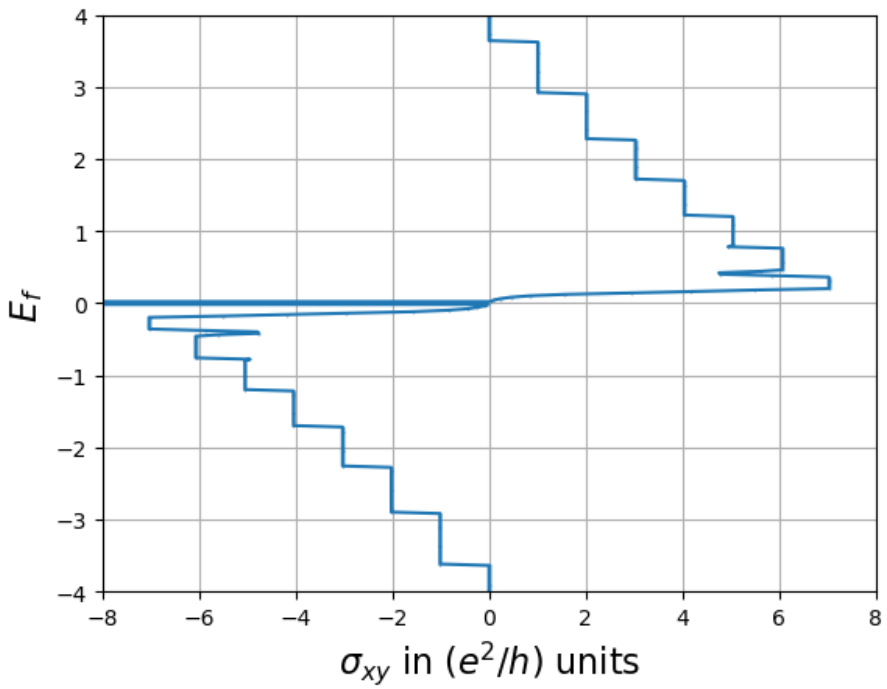

Bibliography

[1] Kishan K Mishra, Aijaz H Lone, Srikant Srinivasan, Hossein Fariborzi, and Gianluca Setti. Magnetic skyrmion: From fundamental physics to pioneering applications. *arXiv preprint arXiv:2308.11811*, 2023.

[2] MS Nicholas Tey, Xiaoye Chen, Anjan Soumyanarayanan, and Pin Ho. Chiral spin textures for next-generation memory and unconventional computing. *ACS Applied Electronic Materials*, 4(11):5088–5097, 2022.

[3] David J. Griffiths. *Introduction to Quantum Mechanics*. Cambridge University Press, illustrated, reprint, revised edition, 2017.

[4] Michael Victor Berry. Quantal phase factors accompanying adiabatic changes. *Proceedings of the Royal Society of London. A. Mathematical and Physical Sciences*, 392(1802):45–57, 1984.

[5] Mahito Kohmoto. Topological invariant and the quantization of the hall conductance. *Annals of Physics*, 160(2):343–354, 1985.

[6] Shilei Zhang. *Chiral and Topological Nature of Magnetic Skyrmions*. Springer, 2018.

[7] Börge Göbel, Ingrid Mertig, and Oleg A. Tretiakov. Beyond skyrmions: Review and perspectives of alternative magnetic quasiparticles. *Physics Reports*, 895:1–28, 2021.

[8] Tsuyoshi Okubo, Sungki Chung, and Hikaru Kawamura. Multiple-q states and the skyrmion lattice of the triangular-lattice heisenberg antiferromagnet under magnetic fields. *Physical Review Letters*, 108(1):017206, 2012.

[9] S. Mühlbauer, B. Binz, F. Jonietz, C. Pfleiderer, A. Rosch, A. Neubauer, R. Georgii, and P. Böni. Skyrmion lattice in a chiral magnet. *Science*, 323(5916):915–919, 2009.

[10] X. Yu, Y. Onose, N. Kanazawa, J. H. Park, J. H. Han, Y. Matsui, N. Nagaosa, and Y. Tokura. Real-space observation of a two-dimensional skyrmion crystal. *Nature*, 465:901–904, 2010.

[11] S. Heinze, K. Von Bergmann, M. Menzel, J. Brede, A. Kubetzka, R. Wiesendanger, G. Bihlmayer, and S. Blügel. Spontaneous atomic-scale magnetic skyrmion lattice in two dimensions. *Nature Physics*, 7:713–718, 2011.

[12] Naoto Nagaosa, Jairo Sinova, Shigeki Onoda, A. H. MacDonald, and N. P. Ong. Anomalous hall effect. *Reviews of Modern Physics*, 82(2):1539–1592, 2010.

[13] Keita Hamamoto, Motohiko Ezawa, and Naoto Nagaosa. Quantized topological hall effect in a magnetic skyrmion crystal. *Physical Review B*, 92(11):115417, 2015.

[14] Y. A. Bychkov and E. I. Rashba. Properties of a 2d electron gas with lifted spectral degeneracy. *JETP Letters*, 39:78, 1984.

[15] G. Dresselhaus. Spin-orbit coupling effects in zinc blende structures. *Physical Review*, 100:580, 1955.

[16] Börge Göbel, Alexander Mook, Jürgen Henk, and Ingrid Mertig. Signatures of lattice geometry in quantum and topological hall effect. *New Journal of Physics*, 19(6):063042, 2017.

[17] Kai Litzius, Ivan Lemesh, Benjamin Krüger, Pedram Bassirian, Lucas Caretta, Klaus Richter, Andrea Krone, Muhammad Kabir, Martin Höing, Simone Finizio, et al. Antiferromagnetic skyrmion crystals: Generation, topological hall, and topological spin hall effect. *Science*, 365(6459):eaaz3868, 2017.

[18] Börge Göbel, Alexander Mook, Jürgen Henk, and Ingrid Mertig. Unconventional topological hall effect in skyrmion crystals caused by the topology of the lattice. *Physical Review B*, 99(9):094421, 2019.

[19] Pratik Sahu, B. R. K. Nanda, and S. Satpathy. Formation of the skyrmionic polaron by rashba and dresselhaus spin-orbit coupling. *Physical Review B*, 106(22):224403, 2022.